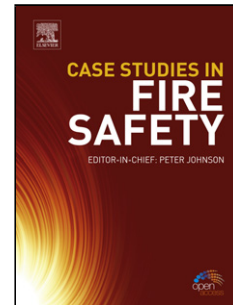


Accepted Manuscript

Title: Review of recent progress in the study of corrosion products of steels in a hydrogen sulphide environment

Authors: Xiangli Wen, Pengpeng Bai, Bingwei Luo, Shuqi Zheng, Changfeng Chen



PII: S0010-938X(18)30244-0
DOI: <https://doi.org/10.1016/j.corsci.2018.05.002>
Reference: CS 7514

To appear in:

Received date: 6-2-2018
Revised date: 26-4-2018
Accepted date: 2-5-2018

Please cite this article as: Wen X, Bai P, Luo B, Zheng S, Chen C, Review of recent progress in the study of corrosion products of steels in a hydrogen sulphide environment, *Corrosion Science* (2018), <https://doi.org/10.1016/j.corsci.2018.05.002>

This is a PDF file of an unedited manuscript that has been accepted for publication. As a service to our customers we are providing this early version of the manuscript. The manuscript will undergo copyediting, typesetting, and review of the resulting proof before it is published in its final form. Please note that during the production process errors may be discovered which could affect the content, and all legal disclaimers that apply to the journal pertain.

**Review of recent progress in the study of corrosion products of steels
in a hydrogen sulphide environment**

Xiangli Wen^{a, §}, Pengpeng Bai^{b, §}, Bingwei Luo^a, Shuqi Zheng^{a, *}, Changfeng Chen^a

^a *State Key Laboratory of Heavy Oil, College of Science, China University of
Petroleum, Beijing, 102249, PR China;*

^b *Department of Mechanical Engineering, State Key Laboratory of Tribology,
Tsinghua University, Beijing, 100084, P. R. China;*

[§] *Xiangli Wen and Pengpeng Bai contributed equally to this work*

^{*} *Corresponding author. Tel.: +86 010 8973 3200. 2870; fax: +86 010 8973 3200*

E-mail address: zhengsq09@163.com; zhengsq@cup.edu.cn

Review of recent progress in the study of corrosion products of steels in a hydrogen sulphide environment

Xiangli Wen^{a, §}, Pengpeng Bai^{b, §}, Bingwei Luo^a, Shuqi Zheng^{a, *}, Changfeng Chen^a

^a *State Key Laboratory of Heavy Oil, College of Science, China University of
Petroleum, Beijing, 102249, PR China*

^b *Department of Mechanical Engineering, State Key Laboratory of Tribology,
Tsinghua University, Beijing, 100084, P. R. China*

[§] *Xiangli Wen and Pengpeng Bai contributed equally to this work*

^{*} *Corresponding author. Tel.: +86 010 8973 3200. 2870; fax: +86 010 8973 3200*

E-mail address: zhengsq09@163.com; zhengsq@cup.edu.cn

Highlights

- Recent progress in the study of corrosion products in a H₂S environment is reviewed.
- Corrosion behaviour of carbon steel in a wet H₂S environment is summarized.
- Polymorphous Fe-S compounds are the corrosion products of steel in H₂S environments.
- The phase transition follows: mackinawite → cubic FeS → troilite → pyrrhotite → pyrite.
- The phase changes of the corrosion product greatly affect the corrosion behaviour of the steel.

Abstract:

In this paper, recent research progress regarding carbon steel corrosion products

and their effects on the subsequent corrosion process in H₂S environments is reviewed. The classification of corrosion products; their dependence on the initiation, growth, and transformation processes; and the corrosion behaviour of carbon steels under wet H₂S environments, and the subsequent corrosion products, are summarized and reviewed. In addition, the basic theory regarding the development of corrosion product films and the relationship between the corrosion products and hydrogen diffusion are discussed. Finally, future research and development directions of this field are proposed.

Keywords: Hydrogen sulphide; Corrosion; Corrosion products; Iron-sulphide compounds; Phase transition

1. Introduction

The distribution of oil and gas resources and consumer markets in China is imbalanced. Most of the oil- and gas-producing areas are far from the major consumer markets, requiring long-distance transportation [1]. Pipelines have become an important means of transporting petroleum and natural gas over long distances because they have the advantages of low cost and large transportation volumes [2]. The extraction and transportation of petroleum and natural gas is highly complicated. Strong corrosive media, such as chloride ions (Cl⁻), carbon dioxide (CO₂), and hydrogen sulphide (H₂S) can quickly degrade the materials used in petroleum equipment in humid environments, seriously threatening the safety and reliability of these systems [3].

H₂S is derived from the degradation of sulphur in sedimentary organic matter by sulphate-reducing bacteria, mainly in deep-sea ecosystems, oil and gas fields, and sewage environments [4]. In the presence of H₂S, many metals are prone to widespread, local, pitting, and linear corrosion [5, 6]. In addition, owing to the “poisoning” effect of H₂S on hydrogen, hydrogen recombination with the metal may occur in a H₂S environment, resulting in the fracture and failure of the material [7]. Oil equipment materials can be severely corroded during service in H₂S-containing environments, resulting in greatly reduced service lifetimes. In addition to causing a great waste of

materials, this significantly impacts safety during production [8].

Currently, corrosion-resistant alloys exist that show good resistance to H₂S corrosion, but they are expensive, so carbon steel is still the most commonly used pipeline material. Corrosion and environmental cracking of carbon steel used in the development of high-sulphur oil and gas fields are major engineering problems in the petroleum and natural gas industry at present that urgently require solutions. The problem of carbon steel corrosion in H₂S environments has attracted considerable attention since the 1940s and has been investigated for nearly 80 years. Most research focuses on the rules and mechanisms of hydrogen damage, such as sulphide stress corrosion cracking (SSC) and hydrogen-induced cracking (HIC), as well as the effect of environmental factors (reaction temperature, partial pressure of H₂S, solution medium, and pH) on the corrosion process [9].

In addition, Canadian scholars in the 1980s found that corrosion products generated in H₂S environments are more complex than those observed in other corrosive environments [10]. Analysing the process considering the corrosion products can provide a way to explore the H₂S corrosion reaction [10]. Subsequently, much research has been performed internationally to investigate the corrosion products. When iron-based alloys are exposed to a wet H₂S environment they will immediately form a corrosion product film. The corrosion products are complex and diverse and tend to exist in mixed crystal forms, primarily non-stoichiometric iron sulphide compounds [11]. Variations in the temperature and partial pressure of H₂S result in large changes in the morphology and crystal structure of the corrosion products. In a low-concentration H₂S environment, mackinawite and cubic FeS are the major corrosion products [12]. In contrast, troilite and pyrrhotite are the main corrosion products in high-concentration H₂S environments, and some researchers have also observed pyrite formation [13]. In recent years, iron sulphide compounds have been confirmed to have some chemical and physical effects on the corrosion and hydrogen damage behaviours of metals, including the impact on hydrogen uptake and the tensile properties of carbon steels [14, 15]. Therefore, it is speculated that the factors affecting the rate of corrosion are mainly related to the degrees of densification and crystal structures of the iron

sulphide compounds [16, 17].

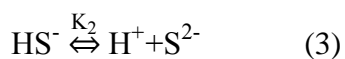
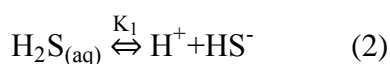
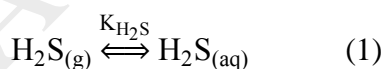
2. H₂S corrosion mechanisms

H₂S is a highly toxic and corrosive substance that is widely investigated in the fields of geoscience, environmental science, and marine systems [18]. Over the last 60 years, the level of knowledge regarding the effects of H₂S on the corrosion of metals in oil and gas production environments has significantly increased since Meyer et al. first identified kansite (now mackinawite) in 1958 [19]. Recently, Smith et al. systematically studied the corrosion mechanisms of carbon steel in a wet H₂S environment and explored the properties and dissolution kinetics of mackinawite [20]. Figure 1 shows the mechanisms of corrosion and hydrogen infiltration into the metal in H₂S environments; a chemical reaction between H₂S and the metal occurs, generating hydrogen molecules [21].

Detailed understanding of sour corrosion mechanisms is an important, but still largely elusive target, especially as it pertains to the interaction between corrosion and corrosion product layer formation. The Nešić group recently investigated the effects of high temperature on the corrosion kinetics of carbon steel and the formation of corrosion product layers in sour environments [22, 23]. Their results showed that increasing the temperature and acid concentration has a synergistic effect on the observed corrosion rate, where the initial corrosion rate increased and reached a steady state over time.

The corrosion mechanism of Fe-based alloys in a wet H₂S environment is as follows:

(i) Ionization reaction of H₂S [24]:



H₂S dissolves in water to generate H⁺ and HS⁻ ions in the first ionization process. The

HS^- ions then undergo secondary ionization to form H^+ and S^{2-} . $K_{\text{H}_2\text{S}}$ and K_i ($i = 1, 2$) are the solubility constants and ionization constants for H_2S , respectively.

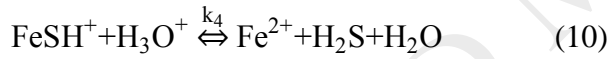
Suleimenov and Krupp [25] studied the solubility of H_2S and obtained the nonlinear expression in equation (4). Suleimenov and Seward [26] proposed equation (5) for the first-order ionization constant of H_2S , and Kharaka [27] published the second-order ionization constant for H_2S (equation (6)). These three nonlinear equations were later verified in many kinetic studies to have the best fits to experimental data.

$$K_{\text{H}_2\text{S}} = 10^{-(634.27 + 0.2709T_k - 0.11132 \cdot 10^{-3} T_k^2 - \frac{16719}{T_k} - 261.9 \log T_k)} \quad (4)$$

$$K_1 = 10^{782.43945 + 0.361261T_k - 1.6722 \cdot 10^{-4} T_k^2 - \frac{20565.7315}{T_k} - 142.741722 \ln T_k} \quad (5)$$

$$K_2 = 10^{-(23.93 - 0.030446T_k + 2.4831 \cdot 10^{-5} T_k^2)} \quad (6)$$

(ii) Anode reactions: the dissolution of iron in acidic solution [28, 29]:



where $\text{FeSH}_{\text{ads}}^-$ and FeSH_{ads} are adsorbed mesophases, k_i ($i = 1, 2, 3, 4$) is the equilibrium constant, and FeS_{ads} is the adsorbed amorphous FeS. These reactions represent the active dissolution of iron based on the intermediate product FeS_{ads} being adsorbed on the surface.

Based on the literature [30, 31], the authors proposed the anodic reaction of iron in the H_2S environment. First, H_2S diffuses to the steel surface and reacts with iron to form FeS (mackinawite). The FeS (mackinawite) scale then dissolves in $\text{Fe}(\text{HS})^+$ and HS^- , and $\text{Fe}(\text{HS})^+$ diffuses away from the metal surface. Finally, more H_2S reacts with the bare steel. This corrosion process continues to produce a very thin ‘‘tarnish’’ of the mackinawite layer, which repeatedly forms and dissolves. In addition, according to

Shoesmith et al., FeSH^+ may combine into FeS_{ads} at the solid-liquid interface (equation (11)), which is called solid-state reaction, or by FeSH^+ hydrolysed to generate Fe^{2+} [10]. Zheng et al. investigated the corrosion mechanisms using potentiodynamic sweeps and comparison with electrochemical modelling [32]. The research results showed that during aqueous corrosion of mild steel, the presence of dissolved H_2S affected both the cathodic and anodic reactions. From this, it can be seen that there is still no consensus on the detailed reaction mechanism based on equations (4) - (6). Many researchers have studied the precipitation kinetics of FeS. Benning et al. experimentally determined an empirical equation for the critical solubility of mackinawite (equation (13)) [33].

$$K_{\text{sp, mck}} = 10^{\frac{2848.779}{T} - 6.347 + \log(K_1)} \quad (13)$$

Rickard proposed that the precipitation rate of FeS is controlled by the concentration of Fe^{2+} and H_2S in the system (equation (14)) [34]:

$$\frac{d[\text{FeS}]}{dt} = k a_{\text{Fe}^{2+}} a_{\text{H}_2\text{S}} \quad (14)$$

where $a_{\text{Fe}^{2+}}$ and $a_{\text{H}_2\text{S}}$ are the activities of Fe^{2+} and H_2S , respectively. These values (formally dimensionless) are represented with units of moles L^{-1} for experimental and practical convenience. The logarithm of k , the theoretical Eigen-Wilkins reaction rate constant, has a value of $7 \pm 1 \text{ L mole}^{-1} \text{ S}^{-1}$.

Harmandas and Koutsoukos described the kinetics of nucleation for amorphous FeS and mackinawite (equation (15)) [35]:

$$R_p = k \sigma_s^m \quad (15)$$

In equation (15), k is the rate constant, σ_s is the relative solution supersaturation with respect to solid phase formation, and m is the apparent order of the reaction.

According to Sun et al., calculating the rate of film formation on the surface of the steel by measuring the concentration of Fe^{2+} is unreliable (both equation (14) and equation (15) are based on this) [36]. In addition, electrochemical corrosion, solid-state chemical reactions, and precipitation of iron sulphide compounds can occur simultaneously, which is not considered in equations (14) and (15). Therefore, the corrosion electrochemical method was used to obtain the kinetic parameters of carbon steel corrosion in an aqueous H_2S environment, elucidate the corrosion and rate control

mechanisms, and obtain an equation for the nonlinear corrosion rate (equation (16)) [30].

$$CR_{H_2S} = A_{H_2S} e^{-\frac{B_{H_2S}}{RT_k}} \ln \frac{c_{b, H_2S} - CR_{H_2S} \left(\frac{\delta_{0.5}^{0.5}}{D_{H_2S} e^{\psi}} + \frac{1}{k_{m, H_2S}} \right)}{c_{s, H_2S}} \quad (16)$$

This is a nonlinear equation with respect to CR_{H_2S} , which does not have an explicit solution, but can be solved using a simple numerical algorithm, such as Newton's gradient method or similar. These are available as pre-written routines in spreadsheet applications or in any common computer programming language. The prediction of CR_{H_2S} depends on a number of constants used in the model which can be found either in handbooks [30] (e.g., D_{H_2S}), calculated from established theory (e.g., k_{m, H_2S}) or determined from experiments (e.g., A_{H_2S} , B_{H_2S} and c_{s, H_2S}). Here, K_{H_2S} is the solubility of H_2S , T_k is the temperature in Kelvin, $a_{Fe^{2+}}$ is the activity of Fe^{2+} , a_{H_2S} is the activity of H_2S , R_p is the precipitation rate, k is the rate constant, $\delta_{0.5}$ is the thickness of the carbon steel, m is the apparent reaction order, k_{m, H_2S} is the mass transfer coefficient for H_2S in the hydrodynamic boundary layer, c_{b, H_2S} is the concentration of H_2S in the liquid phase, c_{s, H_2S} is the concentration of H_2S on the steel surface, A is the surface area of the steel, ψ is the curvature factor of the outer mackinawite, D_{H_2S} is the diffusion coefficient of H_2S , and A_{H_2S} and B_{H_2S} are Arrhenius constants of $1.30 \times 10^{-4} \text{ mol}/(\text{m}^2\text{s})$ and 15.5 kJ/mol , respectively.

(iii) Cathode reaction [28]:



The cathode reactions are constituted by a series of depolarization processes involving H_2S , HS^- , and H^+ . The H^+ ions generated by the ionization of H_2S are ultimately reduced to H_2 .

As part of the overall reaction mechanism [28, 37], in the anode region metallic iron gradually dissolves in solution as Fe^{2+} ions that combine with H_2S to form an FeS precipitate. Simultaneously, H^+ generated by H_2S ionization produces H_2 in the cathode region. However, the presence of H_2S hinders the conversion of hydrogen atoms into

hydrogen molecules, greatly reducing the H_2 generation rate at the metal surface. Some hydrogen atoms diffuse into the steel matrix and form hydrogen molecules.

Hydrogen atoms generated during the corrosion process diffuse into the metal owing to the above-mentioned poisoning effect of H_2S , accumulating in hydrogen traps (such as dislocations, grain boundaries, and inclusions) and gradually form hydrogen molecules, resulting in hydrogen blistering (HB) or hydrogen-induced cracking (HIC). When carbon steel is simultaneously subjected to external forces, mechanical failures such as sulphide stress corrosion cracking (SSC), hydrogen-induced cracking (HIC), stepwise cracking (SWC), and stress-oriented hydrogen induced cracking (SOHIC) may occur, as shown in Figure 2 [38, 39]. The nature and occurrence of these processes depend on the strength, microstructure, and process conditions used to manufacture the carbon steels.

3. Corrosion products on the surface of carbon steels in a H_2S environment

The characteristics of the corrosion product film are important for determining the theoretical models of the corrosion mechanism and developing new corrosion inhibitors. Some studies have shown that, under certain conditions, the corrosion products play a role similar to that of stainless steel passivation films, which can decrease damage to the metal; this is commonly known as corrosion protection [40-44]. The corrosion products formed on a steel surface in a H_2S environment mainly consist of non-stoichiometric polymorphous iron sulphide compounds. At least nine different solid phases with sulphur and iron have been identified; their compositions and structural information are shown in Table 1 [45].

For most crystal structures of the iron sulphide compounds produced in the H_2S corrosion environment, the microstructure of the corrosion products is closely related to the environment. Mackinawite and cubic FeS are commonly observed corrosion products at normal temperature and low H_2S pressure [46]. Under high temperature and high H_2S pressure, troilite, pyrrhotite, pyrite, and other crystalline iron sulphide

compounds may form [47]. The most common corrosion product formed during the practical application of carbon steels is amorphous ferrous sulphide; because of its amorphous structure, structural information cannot be obtained using X-ray diffraction (XRD). In the early days, Rickard identified amorphous FeS as a short-lived, black precipitate with the formula $\text{Fe}(\text{HS})_2$, which acts as a base compound for the formation of other iron sulphides [48]. It was later claimed that amorphous FeS essentially contains mackinawite nanocrystals that are too small to be detected by XRD and is mistakenly defined as amorphous FeS [49]. In addition, previous research has shown that mackinawite is the first product formed in the H_2S environment [47]. Tetragonal FeS_m (mackinawite) is considered the initial and most important corrosion product of carbon steels in the H_2S environment.

Bai et al. systematically studied the corrosion products on the surface of X52 pipeline steels (contains 0.13 wt.% C) under different temperatures and partial pressures of H_2S via corrosion deposition experiments [50, 51]. They observed that even after a very short period (10 s), carbon steel in contact with H_2S showed appropriate nucleation conditions for forming iron sulphide compounds. The average height difference reached 50-100 nm after corrosion for 10 s, where the deepest trench, which was thought to be the grain boundary, was ~ 100 nm. In addition, when the surface height difference reached approximately 100 nm, the potential difference between the ferrite and carbide accelerated the dissolution of iron, and the grain boundaries preferentially corroded, as shown in Figure 3 [50]. Nano-sized iron sulphide compounds were identified as the initial corrosion product. The morphologies of corrosion products with different crystal configurations are quite different. Amorphous iron sulphide compounds have an irregular morphology; tetragonal mackinawite often shows a flake-like morphology; cubic FeS has a perfect octahedron or truncated octahedron shape; pyrite forms spherical particles; troilite has a six-prismatic, acicular; or flower-shaped structure, and pyrrhotite shows a super-structure, as shown in Figure 4 [51].

Shoesmith et al. showed that at 21 °C and pH = 4, mackinawite simultaneously formed on the metal surface by both solid-state and deposition reactions, followed by the nucleation of cubic FeS and troilite on the iron surface [52]. Smith noted that the rupture of mackinawite film led to the nucleation and growth of other new Fe-S phases

[53]. Zheng et al. showed that in sulphur-containing H_2S environments, the corrosion rate of carbon steel increases linearly with increasing temperature when the temperature is below the melting point of sulphur. At higher temperatures, the formed corrosion product film is thicker, and the adhesion between the film and the metal substrate is weaker than that formed at lower temperatures. XRD results also showed that the corrosion products consisted of cubic FeS and a small amount of tetragonal FeS, and the temperature had little effect on the chemical composition of the corrosion products [54]. Qi et al. studied the corrosion behaviour of carbon steel exposed to H_2S at different temperatures by measuring the weight loss and undertook electrochemical measurements, scanning electron microscopy (SEM), and XRD. With increasing temperature, the corrosion rate first increases and then decreases; a finer, denser corrosion product film was formed at higher temperatures, which was an effective protection against corrosion of the carbon steel [55].

Compared to mackinawite, hexagonal troilite and pyrrhotite are more common corrosion products in high-temperature and high-pressure environments. Many scholars have discussed the restrictive growth mechanism of hexagonal crystal iron sulphide compounds for nearly 40 years. At present, it is generally accepted that in excess elemental sulphur, Fe^{2+} penetrates the sulphide film and migrates to the outside, resulting in the formation of a sulphur-rich and iron-deficient corrosion product [56]. The morphologies of corrosion products with different crystal configurations differ greatly. For example, the grains of mackinawite-type corrosion products are small and mostly flaky and can be removed by ultrasonic treatment in alcohol. However, hexagonal corrosion product crystals are large and tightly bonded to the substrate, requiring the use of a blade to peel them off [15].

Amri et al. presented a simple solid-state model for the growth of iron sulphide compounds that can allow the handling of solid-state transport and both internal and interfacial reactions [57]. Although approximate, the model successfully describes the parabolic film growth regime. It has also been shown that the proposed model can, to some extent, reproduce results of recent corrosion experiments showing parabolic iron sulphide film growth and mass loss. Herbert summarized previous studies and developed a model for the nucleation and growth of mackinawite [58]. A schematic diagram of the growth of iron sulphur compounds on the steel has been summarized.

Initially, by solid-state reaction or local deposition reactions, nanoscale mackinawite films form on the surface of carbon steel. After continuous dissolution and recrystallization of mackinawite, a thick product film forms at the interface. Subsequently, the corrosion product film delaminates because of internal stresses, resulting in the production of pits. Finally, troilite and pyrrhotite appear owing to higher cation concentrations in the pits and kinetic conditions appropriate for stable phase nucleation.

The thermodynamic properties of corrosion products with different crystal structures also vary. It has been shown that pyrrhotite (including troilite) and pyrite are thermodynamically stable, mackinawite and greigite are metastable, and cubic FeS is highly unstable [45]. The standard Gibbs free energy ($G_{298.15}^0$) of pyrite is approximately -160.06 kJ/mol, mackinawite is approximately -93.3 to -100.07 kJ/mol, and pyrrhotite is between -101.95 and -114.5 kJ/mol [59]. In 2015, the Nešić group published a preliminary prediction model for the corrosion products in the aqueous H₂S environment using Pourbaix (E_h-pH) diagrams based on thermodynamics principles and data from previous studies [60]. They investigated the effect of the ambient temperature and H₂S pressure (Figure 5), which are important for predicting the composition of the corrosion products. In 2017, Zhang et al. explored the relationship between the external environment and corrosion products based on many previous experimental results. The thermodynamic model was used to predict the formation conditions for mackinawite and pyrrhotite, and its accuracy was further verified by comparison with experimental data, as shown in Figure 6 [61]. Subsequently, Wen et al. calculated the thermodynamic parameters of mackinawite and pyrite over a range of temperatures using density functional theory (DFT). It was observed that the Gibbs free energy of both mackinawite and pyrite decreased significantly with increasing temperature, and the degree of pyrite reduction was more obvious, indicating that pyrite was more stable under high-temperature conditions than the other phases [62]. In the following sections, the research background and status of several common corrosion products in the H₂S environment are discussed in more detail.

3.1 Mackinawite

Mackinawite is the most common natural source of iron sulphide compounds [63]. This material has been widely studied in geoscience, environmental science, and other

fields. In addition, mackinawite is the most common corrosion product in the H₂S environment [47, 64]. Mackinawite occurs in a tetragonal crystal structure; iron atoms are surrounded by four equidistant sulphur atoms forming a tetrahedral structure by coordination, where four iron atoms are connected to form a regular tetragon [18, 65]. The Fe(II) on the surface of the mackinawite easily loses electrons when exposed to an oxidizing substance, causing the mackinawite to be very susceptible to oxidation [66]. When mackinawite was initially characterized by dissolving it in a strong acid such as HCl, a small amount of elemental sulphur was observed in solution, resulting in the conclusion that it was an iron-rich iron sulphide. However, in the last ten years, the academic community has considered that mackinawite is not an iron-rich sulphide, but rather a compound with a stoichiometric balance of sulphur and iron [67]. In recent years, foreign scholars have designated amorphous FeS as nanocrystalline mackinawite because two-dimensional lattice fringes of mackinawite can be detected with high-resolution electron microscopy [49, 65]. Recently, Genchev et al. identified mackinawite in a H₂S-containing environment and observed changes in the mackinawite Raman spectra over time [68]. The observed spectral changes may be attributable to restructuring, defect healing, and defect formation within the sulphur sub-lattice, possibly caused by minor oxidation of some of the Fe²⁺ in mackinawite. The observed aging clearly implies structural changes on the local level.

3.2 Cubic FeS

Cubic FeS was first discovered by Médicis [69] and Takeno et al. [70]. It mainly exists in the H₂S corrosive environment of iron-based alloys and has recently been found in magnetic bacteria [71]. Cubic FeS is a sphalerite structure with sulphur atoms arranged at the nodes of the face-centred-cubic lattice, with the iron atoms occupying half the tetrahedral centre [72].

At temperatures below 92 °C and a pH of 2-6, Fe (0) and S (-II) react in the aqueous phase to produce cubic FeS [73]. Compared to other iron sulphide compounds, cubic FeS is a metastable structure that undergoes phase transitions within a few days

at room temperature. By monitoring the reactants and products, Murowchick and Barnes showed that an environment with pH = 4-5 and a temperature of 35-60 °C is favourable for the nucleation of cubic FeS, which is derived from Fe (0) and S (-II) and competitive reactions between Fe^{2+} and S^{2-} [73]. However, the exact formation mechanism of cubic FeS is not yet clear. Cubic FeS in the sphalerite structure includes the $\text{Fe}_4\text{S}_6^{2-}$ subunit, and the $[\text{Fe}_4\text{S}_6(\text{H}_2\text{O})_4]^{2-}$ groups may be a necessary precursor in solution [74]. Cubic FeS has not been found in nature, possibly owing to its short lifetime.

3.3 Pyrrhotite and troilite

Pyrrhotite is the most common Fe-S mineral in the solar system. It has a variety of super-structures based on the basic NiAs crystal configuration. Solid solutions contain iron vacancies, according to the different lattice constants classified into 4C, 5C, 6C, 5T and so on [75]. Figure 7 shows the structure of pyrrhotite projected onto the (001) crystal plane of 1C, 2C, 4C and 5C [76]. Some scholars have developed the statistics on the literature pertaining to the generation of pyrrhotite-type corrosion products. These studies showed that pyrrhotite, a corrosion product with a hexagonal structure, is generally found on metal surfaces with a longer service life or in high-pressure H_2S environments; this structure does not nucleate easily in low-temperature and low-pressure H_2S environments. When pyrrhotite is formed, the corrosion rate of steel is generally lower [19, 51, 77-89], as shown in Table 2. Wikjord et al. found that a 1.5-MPa H_2S environment produced pyrrhotite with a hexagonal micro-morphology [81].

Troilite belongs to the pyrrhotite crystal system and possesses a NiAs-type super-structure at room temperature, where $a = \sqrt{3}A$ and $c = 2 C$ (A and C are the crystal constants of NiAs) [90, 91]. The phase of this structure is called low-temperature troilite and undergoes spin-inversion transition (α -phase transformation) at 140 °C and first-order phase transformation (β -phase transformation) at 315 °C and is converted to NiAs unit cells (1C), as shown in Figure 8 [92, 93]. In addition, troilite has been synthesised

with a MnP-like structure under high-temperature and -pressure conditions [94]. Singer et al. found that troilite is acicular in H₂S environments, as shown in Figure 9 [95].

3.4 Greigite and pyrite

Skinner discovered greigite for the first time in the Miocene lakes of California [96]; it is commonly found in microbial environments and allows magnetic bacteria to arrange directionally in a magnetic environment [97, 98]. Greigite is not commonly found in the Fe-H₂S-H₂O system, although it has been reported in the literature that it may exist in oxygen-containing environments. However, no relevant reaction mechanism has yet been proposed.

Greigite has an anti-spinel structure (A(AB)₂S₄) [99], similar to ferrous oxide. The unit cell contains 56 atoms (24 iron atoms and 32 sulphur atoms). The Fe atoms are divided into two sub-lattices, where eight iron atoms occupy tetrahedral positions (A positions), 16 iron atoms occupy octahedral positions (B positions), Fe (II) is in the tetrahedral A positions, mixed Fe(II) and Fe(III) atoms are in the octahedral B site, and sulphide ions are in a cubic lattice [72].

Pyrite has a cubic crystal structure, similar to that of NaCl [100], and is the largest Fe-S mineral found in the earth's crust. Pyrite has been widely investigated, especially by a British group led by David Rickard, who synthesized strawberry pyrite crystal grains in an Fe-H₂S-H₂O system [101]. In related reports of H₂S corrosion, pyrite is often found in high-sulphur or high-temperature environments [102], but it has not been observed in low-H₂S environments. The corrosion products with different crystal structures generated in different environments are summarized in Table 2 [33, 50, 51, 61, 78-89].

4. Phase transitions of corrosion products and other iron sulphides

Iron sulphide compounds belong to a special category of metal sulphides with a large number of crystal systems with complex structures; in addition, these compounds show mutual transformation between different phases [103, 104]. Different iron

sulphide crystal structures have very different thermodynamic and physical properties. Changes in the trace S-Fe compositional ratio result in changes in the crystal structure. Even with the same S-Fe ratio, different crystal structure types can occur, which show significantly different optical, electrical, and catalytic properties. These findings have an important impact on the field of corrosion, as well as photovoltaics, thermoelectrics, lithium batteries, and other new energy research hot spots [105-108]. Herbert [58] summarizes the Fe-S phase diagram obtained by research scholars. It can be found that there are many phase transitions in the iron-sulphide system as a function of iron-sulphur ratio and temperature.

4.1 Phase transitions of sulphide compounds

Lennie used in-situ XRD to study the phase transition behaviour of laboratory-synthesized mackinawite under an inert gas environment [109]. The results showed that mackinawite was rapidly converted to greigite (Fe_3S_4) after being heated to 100 °C; further in situ heating transformed Fe_3S_4 to pyrrhotite and magnetite. Bhargava also used in situ high-temperature XRD to study pyrite phase transitions in different environments, as shown in Figure 10 [110]. Hematite ($\alpha\text{-Fe}_2\text{O}_3$) and magnetite (Fe_3O_4) were observed when pyrite was heated in low-pressure air. Pyrrhotite was formed by heating in a nitrogen/argon environment. When heating in carbon dioxide, pyrrhotite was initially formed, resulting in the formation of hematite ($\alpha\text{-Fe}_2\text{O}_3$) and magnetite (Fe_3O_4) with increasing temperature, mainly owing to the decomposition of carbon dioxide at high temperatures into oxygen and carbon monoxide. Bhargava used in situ XRD to study pressure-induced phase transformation of single-crystal troilite samples [110]. The results showed that at 25 °C and 3.4 GPa, the troilite was converted into a MnP-type crystal with a hexagonal unit cell (Pnma space group). Increasing the pressure to 6.7 GPa resulted in an unknown crystal structure and a reduction in the volume of approximately 9%, and the lattice constant ratio (C/A) substantially decreased. Ono et al. used first-principles simulations to calculate pressure-induced phase transformations of troilite and observed many new phases, such as FeS with a

diamagnetic MnP structure, which was stable under low-pressure conditions. Under high pressure (40-135 GPa), a non-magnetic MnP structure of FeS was observed which was stable at 135 GPa, as shown in Figure 11 [111]. Subsequently, Using DFT calculations, Wen et al. showed that mackinawite is converted to pyrite at approximately 147 °C (420 K) [62].

4.2 Phase transformation of corrosion product in H₂S environment

4.2.1 Temperature change

The temperature greatly affects the phase transition and subsequent crystal structure of materials. Smith and other researchers showed that low-alloy steel in H₂S environments, first forms mackinawite on the metal surface, and when the temperature reaches 170-200 °C, pyrrhotite nucleates on the mackinawite matrix surface [112, 113]. Sun et al. showed that mackinawite first forms on the metal surface by a solid phase reaction. Once the thickness of the iron-sulphur film increases to a critical value, cracking occurs; at lower pH values, cracking occurs more quickly. The metal matrix dissolves rapidly via cracks and holes in the protective film, leading to an increase in the local Fe²⁺ concentration; a supersaturation of Fe²⁺ results in the deposition of FeS to form cubic FeS, troilite, or pyrrhotite [114]. Some scholars have shown that at 140-160 °C, the mackinawite will decompose to form other iron sulphides, which are mainly transformed into troilite or pyrrhotite [11, 52, 79]. Wikjord et al. also found that mackinawite shows a phase transition in solutions with pH ≤ 5, H₂S partial pressure up to 20 bar, and temperature of 80-180 °C [81]. The order of this phase transitions was mackinawite → cubic FeS → troilite → pyrrhotite → pyrite.

Bhargava also conducted temperature-induced phase transition experiments on single-crystal troilite samples and found that troilite was converted to a MnP-type crystal at 147 °C (420 K) under atmospheric pressure. This crystal belongs to the Pnma space group and has a hexagonal unit cell. Continued heating produced a secondary transformation, resulting in the formation of a NiAs-type structure (P63/mmc space group) [110]. Zhou et al. studied X52 carbon steel in an H₂S aqueous solution

containing 5 wt.% NaCl; the corrosion products transformed from mackinawite + troilite to mackinawite + pyrrhotite with increasing temperature [115]. Qi et al. studied the corrosion behaviour of carbon steel exposed to H₂S at different temperatures and found that, with increasing temperature, the originally formed mackinawite in the corrosion product film was converted to cubic FeS [55].

Liu et al. conducted high-temperature and high-pressure immersion tests in an autoclave to study the corrosion behaviour of X52 pipeline steel in aqueous solutions with high concentrations of H₂S [116]. The results showed that with increasing temperature and H₂S concentration, the order of phase transformation was mackinawite → troilite → pyrrhotite, where the microstructure and stability of the corrosion products had an important effect on the corrosion rate. Bai et al. studied the phase transition characteristics of corrosion products using high-resolution transmission electron microscopy (HRTEM) and found that iron sulphide compounds in low-temperature Fe-H₂S-H₂O environments evolved as follows: mackinawite and a small amount of cubic FeS → troilite and a small amount of greigite → troilite and a small amount of pyrite; the mackinawite and cubic FeS can be transformed into greigite, as shown in Figure 12 [117].

Li et al. studied the phase transition behaviour of un-oxidized and surface-oxidized mackinawite under He and H₂S conditions using DFT calculations and experimental methods. The DFT results show that the transition from mackinawite to hexagonal pyrrhotite is endothermic, but the phase transitions to greigite, marcasite, and pyrite are exothermic reactions. The experimental results show that the un-oxidized mackinawite was converted to pyrrhotite in both He and H₂S environments and the structure of the oxidized mackinawite surface depended on the degree of oxidation. For low degrees of oxidation, only Fe²⁺ was converted to Fe³⁺, resulting in a mixture of greigite and mackinawite as products. For higher degrees of oxidation, the surface of Fe was oxidized to Fe³⁺, forming pyrite, as shown in Figure 13 [118].

Subsequently, Esmaeely et al. performed cathodic potentiodynamic sweeps of different iron sulphide surfaces in deoxygenated aqueous H₂S solutions with different pH values. Cathodic sweeps on pyrrhotite showed an extra feature at the lower current

densities obtained at more positive potentials, identified as the transformation of pyrrhotite into troilite [119].

4.2.2 Pressure change

Taylor et al. showed that the phase transition behaviour of monosulphides at 160 °C and 1.8 MPa H₂S occur as follows: mackinawite → greigite + pyrrhotite → pyrite; troilite → pyrrhotite → pyrite [120]. Smith reported that mackinawite was the main H₂S corrosion product at low temperatures and H₂S partial pressures, which gradually transformed into pyrrhotite with increasing temperature and H₂S partial pressure, where the boundary between these phase is a straight line with a negative slope [121]. Ning et al. developed a comprehensive thermodynamic model to predict the corrosion products of the Fe-H₂S-H₂O system [122]. When the partial pressure of H₂S increased from 0.0001 to 10 bar, the boundary of the mackinawite formation region shifted greatly from pH 6.0 to 3.3, revealing that the formation of a mackinawite layer is thermodynamically favoured at higher H₂S partial pressures. In addition, with increasing H₂S partial pressure, pyrrhotite is easily transformed into pyrite.

Summarizing the previous research, under low-temperature conditions, the sequence of phase transformations for pressure-induced troilite was troilite → diamagnetic MnP phase → monoclinic phase → non-magnetic MnP phase → pmmn phase.

5. Role of corrosion products in corrosion science

5.1 Effect of corrosion product film on the subsequent corrosion process

The protective role of corrosion product film has always been an important research topic in the field of corrosion science. Corrosion product film has been linked to the corrosion resistance of metals because it can promote or inhibit further corrosion. Some scholars call corrosion product film a passivation layer. Ma et al. studied the effect of iron sulphide compound film on the corrosion process using an

electrochemical method and showed that corrosion product film formed an ionic barrier when the H₂S concentration was less than 0.00128 g/L with pH 3-5 [28]. On the other hand, a porous corrosion product film is less protective than a dense film and may also increase the corrosion rates if the corrosion product has significant electrical conductivity and galvanic cells between the steel and the corrosion product film are established [44]. Table 3 summarizes the corrosion rates of different corrosion products [123-128].

Sardisco et al. studied the structure of the corrosion products formed under different H₂S partial pressures in a NaCl-free environment and found that the mackinawite was porous and could not protect the metal, resulting in a higher corrosion rate [46]. Liu et al. studied the corrosion behaviour of X52 pipeline steel in H₂S solutions through immersion corrosion test [129]. The results showed that due to the different corrosion mechanisms, the structure and stability of the corrosion products have a significant influence on the corrosion rate. The corrosion resistance of the corrosion products increased as follows: mackinawite < cubic FeS < troilite < pyrrhotite. Subsequently, this research group also showed that the main corrosion products changed from iron-enriched mackinawite to sulphur-rich pyrrhotite with increasing immersion time [130]. The corrosion product film showed two layers, a fine-grained iron-rich inner layer and a columnar-grained sulphur-rich (outer layer). The corrosion product film was formed by a combination of outward diffusion of Fe²⁺ ions and inward diffusion of HS⁻ ions. After a long immersion time, changes in the composition of the corrosion products and compaction of the corrosion layer resulted in a decrease in the diffusion coefficient, where the formed double-layer corrosion film showed an effective diffusion barrier effect.

Zhang et al. studied the crystal structure and micromorphology of corrosion products under H₂S environmental conditions using XRD, SEM, and TEM [89]. In addition, studies have shown that the existence of pyrrhotite somewhat reduces further corrosion of carbon steel. Bai et al. used electrochemical impedance spectroscopy experiments to show that a uniform corrosion product film increased the charge transfer resistance [42]. Subsequently, hydrogen permeation experiments showed that the

hydrogen permeation curve of pyrrhotite-coated carbon steel had a significantly lower peak than that of bare steel. Thus, pyrrhotite could behave as a hydrogen permeation barrier in H₂S-containing environments. Qi et al. performed a slow strain rate tension (SSRT) and showed that a uniform corrosion product film reduced the plastic loss of steel [14]. Zhou et al. showed that, under acidic conditions, the hydrogen permeation current is lower than in neutral solutions. A high peak value and slow decay was observed in a high-pressure H₂S environment, and a steady low-peak-type curve was observed at atmospheric pressure; this may be related to the different types of surface corrosion products, as shown in Figure 14 [15, 111].

Li et al. investigated the effect of H₂S content and corrosion product coverage on the hydrogen permeation of pipeline steel by electrochemical methods [131]. The results showed that the corrosion behaviour of pipeline steel at different H₂S contents was mainly affected by the structure and density of corrosion products. The average corrosion rate of the pipeline steel first increased with H₂S content and then decreased. The hydrogen permeation behaviour of pipeline steel was mainly affected by the concentration of H₂S molecules in solution, the adsorption of HS⁻, and the structure and density of the corrosion products. Zheng et al. designed and built a novel experimental set-up to investigate the effect of an iron sulphide layer grown during H₂S corrosion of carbon steel [132]. The results showed that the balance between the precipitation and undermining processes of iron sulphide and its effect on corrosion depended on environmental parameters, such as temperature, pH, and flow rate. A protective corrosion product layer and low corrosion rate were observed at high pH, high temperature, and low flow rate due to the precipitation of a dense corrosion product layer. Wang et al. studied the effect of temperature on the hydrogen permeation of pipeline steel in a wet H₂S environment [133]. The steady-state permeation current density, steady-state flux, and permeation rate increased with increasing temperature. The corrosion rate was highest at 35 °C as confirmed by electrochemical tests. This study showed that the corrosion process was controlled by the cathode reaction. Hydrogen permeation under wet H₂S conditions was influenced by both the corrosion rate and type of corrosion products. Through electrochemical tests, Zhao et al. found

that the corrosion product film on the surface of carbon steel reduced the occurrence of pitting corrosion [134]. In addition, the corrosion resistance of carbon steel also improved when the immersion time was extended and corrosion products were increased. Navabzadeh et al. also found that a dense protective layer formed on top of the pyrrhotite layer on the specimen exposed to an aqueous H₂S solution with 1 wt.% NaCl [135]. Thus, dissolution of the previously formed pyrrhotite layer slowed significantly, and no localized corrosion was observed. These studies show that the Fe-S corrosion product film affects the subsequent corrosion process.

5.2 Theoretical studies of the corrosion product film

For many years, corrosion products were only qualitatively considered as cationic precipitates and used for the backward derivation of the mechanism of corrosion reactions. Nešić's research group at Ohio University developed a new electrochemical model for simulating the effect of pH₂S, flow, temperature, and pH on the corrosion of mild steel in an H₂S environment in the absence of iron sulphide layers [32]. Yildiz's research group at the Massachusetts Institute of Technology applied the theory of metal passivation to the theoretical study of corrosion products [58, 136]. A point defect model was developed and using simulation methods a reaction model was developed for the Fe-H₂S-H₂O system in the presence of iron sulphide compound films, along with a kinetic Monte Carlo (kMC) model of the interfacial reactions in the multi-layer film. This may be the most important advance in H₂S corrosion theory in recent years. Although the results of such simulations have not yet been confirmed experimentally, the Fe-S passivation film theory provides a new direction for future research. Herbert [58] summarized the corrosion mechanism for the basic unit of an iron sulphide compound film. Most of the key atomic steps are described, such as ion diffusion, surface change (interfacial charge transfer reaction), and the formation of vacancies under reducing conditions. In addition, it also depicts other important phenomena affecting the stability of the corrosion product film.

Krishnamoorthy [136] used a multi-pass passivation film simulation model (40

nm × 40 nm × 320 nm) for theoretical studies. The result shows the evolution of a multi-layer iron sulphide film on a metal in a sulphidizing environment including mackinawite, pyrrhotite, and pyrite. First, the representative result from the kMC model at the film-environment interface showing the film dissolution processes and vacancy dynamics. The result also shows the topography of the film surface, indicating the different terrace and pitting regions. Then, the output from the kMC model for H₂ evolution in the mackinawite phase, indicating atomic-scale spatial distribution of H₂ evolution events in the passive film. Finally, the distribution of vacancy agglomeration at the metal-film interface, resulting in delamination of the passivation film.

5.3 Relationship between corrosion product film and hydrogen diffusion

The H₂S partial pressure is a major indicator of the type of corrosion product that will be formed, and hydrogen embrittlement is the predominant problem related to H₂S corrosion. However, the effects of corrosion products on hydrogen embrittlement have not been extensively studied. Omura et al. studied the hydrogen content in corroded samples by thermal desorption spectrometry (TDS) [137]; the hydrogen content in the steel decreased with increasing H₂S partial pressure from 0.1 MPa to 1 MPa. In addition, as the ambient temperature increased from 24 °C to 65 °C, the H evolution rate inside the steel also decreased. Wallaert et al. investigated the effect of corrosion products on hydrogen diffusion via hot extraction techniques and found that the corrosion products acted as physical barriers to hydrogen diffusion [123].

Krishnamoorthy used DFT calculations to show that the presence of monoatomic hydrogen interstitials and interlayer molecular H₂ interstitials reduced the ultimate tensile strength and modulus of elasticity of mackinawite by more than 90%, in which atomic hydrogen had a certain strengthening effect [138]. Atomic H interstitials led to in charge transfer to the mackinawite layers and created dipolar attractive interactions among layers, enhancing the mechanical properties, which is consistent with the MoS₂ results [139]. However, molecular H₂ interstitials induced only steric repulsion that weakened existing attractive van der Waals bonding, as shown in Figure 15.

5.4 Corrosion of carbon steel by S-containing deposits and suspended matter

When corrosion products are formed, multi-phase flow in a pipeline promotes delamination of corrosion products from the substrate, which become suspended in the fluid or deposited on the bottom of the pipeline. In particular, in horizontal tubes, these iron sulphide compounds can cause corrosion of the steel (the extent of which depends on the crystal structure of the corrosion product phase).

Sulphur-containing deposits, unlike sand deposition, not only promote the formation of a concentration cell but also can cause galvanic corrosion of the metal, which is related to the semiconducting characteristics of iron sulphide compounds [140]. King et al. used corrosion weight loss methods to prove that pyrite deposits result in the most severe corrosion on steel compared to the minor effects of mackinawite and pyrrhotite, owing to differences in the sulphur content, as shown in Figure 16 [141]. Zhang et al. showed that the corrosion rate of carbon steels with ferrous sulphide deposits increases with increasing thickness of the deposits, as shown in Figure 17 [142, 143]. In addition, exfoliated corrosion products may reduce the effectiveness of the corrosion inhibitor, mainly because corrosion inhibitors are adsorbed on the surface of the deposits [144]. There has been less research on sulphur suspended matter. Bai et al. found that suspended corrosion products can weakly adhere to the steel surface; the adhered FeS acts as a cathode, leading to electrochemical corrosion. Anodic dissolution occurs on the carbon steel substrate, and cathodic reduction occurs on the FeS. Eventually, the combination of FeS and H₂S can result in severe corrosion of carbon steel in the H₂S environment [145].

6. Concluding remarks: future research

This review summarizes the research progress of many scholars in recent decades on the types of corrosion products of carbon steel in H₂S environment and the mechanisms by which the corrosion products affect the subsequent corrosion process. The classification and characteristics of corrosion products and their dependence on the

environment, the nucleation conditions, the growth and transformation of corrosion products, the influence of corrosion products on further corrosion of carbon steel, the mechanisms by which the corrosion products affect the corrosion behaviour of carbon steels under wet H₂S conditions, the theoretical study of the fundamental properties of the corrosion product film and the relationship between the corrosion products and hydrogen diffusion are summarized and reviewed.

The corrosion products formed on a steel surface in a H₂S environment mainly consist of non-stoichiometric polymorphous iron sulphide compounds. The corrosion products that have been discovered to date include mackinawite, cubic FeS, troilite, pyrrhotite, smythite, greigite, pyrite, and marcasite. Some studies showed that these corrosion products can effectively inhibit subsequent corrosion. However, there are still several challenges that need addressing. The first is the nucleation process of the corrosion product film, where there is a lack of in-situ data. Only a few articles studied the initial corrosion behaviour; due to the violent reaction of the metal with hydrogen sulphide, the nanoscale nucleation process was not accurately described in previous studies. In a recent study, it was found that simulation of this system was a good method; however, the existing database of iron sulphide compounds was found to be insufficient. The second point challenge involves identifying whether the evolution of the corrosion product is due to dissolution recrystallization or a phase change process. This topic was already of interest in the 1980s, but little information about the phase change process was known; most reports simply showed that the product type changed with time. The third topic is the protection of carbon steel by corrosion products, which involve surface ion transport and surface defect effects. Therefore, detailed knowledge cannot be obtained only from electrochemical methods and corrosion rates. This topic needs further study considering the inherent properties of the sulphides, including the interfacial behaviour of different iron sulphides in solution, the mechanism of dissolution recrystallization, and the mechanical properties of iron sulphide at the micro- and nanometer scales. These challenges should all be considered and resolved in future research.

To date, the fundamental nucleation and phase transformation mechanisms of the

corrosion products in the Fe-H₂S-H₂O system have not been clarified, and the thermodynamic and kinetic behaviour of corrosion product formation and transformation needs further study. Previous theoretical calculations and experimental studies yielded, thermodynamic and kinetic parameters of the corrosion products, and enhanced understanding of the phase transformation process of polymorphous Fe-S compounds. These findings also provided a theoretical basis and data to support predictions regarding the corrosion products in the Fe-H₂S-H₂O system and helped improve the Fe-S phase diagram.

In addition, experimental results showed that the corrosion product film influenced the corrosion process of carbon steel, although this topic was predominantly studied from the macroscopic point of view considering that a dense layer has a protective effect. However, the interaction between H₂S and corrosion products of different crystal structures, microscopic adsorption/desorption mechanism, and further formation of corrosion products are still unclear. By combining macroscale experimental results with microscale theoretical calculations, the influence of the corrosion product film on subsequent corrosion can be analyzed; this provides an important basis for understanding the corrosion protection of carbon steel and improving its performance.

Furthermore, there is still no theoretical basis for the mechanism of surface spalling after interaction between H₂S and the passivation film. A current research focus is investigating the effect of the corrosion product film on further corrosion at the atomic scale. In addition, it is important to theoretically calculate the volume change before and after interaction of the corrosion product film with H₂S and analyze the possibility of surface flaking and phase changes. Combining this knowledge with experimental results is expected to reveal the mechanism of further corrosion.

Finally, one of the major risks of H₂S corrosion is hydrogen embrittlement; however, the effect of the corrosion products on hydrogen embrittlement is rarely studied. The dissociative adsorption of H₂S results in two isolated H atoms being adsorbed on the corrosion product surface, where the H atom can migrate over the surface and diffuse into the bulk. Therefore, the diffusion mechanism of hydrogen atoms from the surface of the corrosion products to the inner layer still needs to be

clarified. Studying the optimal diffusion paths and controlling the diffusion energy barrier of the H atoms provides direct data for the diffusion of H atoms into the inner layer and accumulates at the defects, which can reveal the mechanism behind the damage caused to the corrosion product film by H atoms.

Experimental and theoretical studies can provide information about the order of anti-H₂S corrosion ability and reaction mechanism for corrosion products with different crystal structures. Therefore, it will be possible to clarify the corrosion product growth process and the influence of the different crystal corrosion products on H₂S corrosion. In addition, a technique for rapidly depositing a corrosion product film with good H₂S corrosion resistance on the surface of carbon steel could be realized. Future studies are expected to explore the adaptability of carbon steel in H₂S environment, provide technical support for exploring the H₂S corrosion mechanisms and improving the corrosion resistance of carbon steel, and provide a theoretical basis for related scientific research and industrial processes.

Acknowledgements

This work was financially supported by the Natural Science Foundation of China (No. 51671215) and the National Postdoctoral Program for Innovative Talents (No. BX201700132). The authors are grateful for helpful discussions with Dr. Luo Yue.

References:

[1] L.I. Helin, Hot topics in study and application of steel line pipe for natural gas transportation, *Chin. Mech. Eng.* 3 (2001) 035.

[2] R.G. Santos, W. Loh, A.C. Bannwart, O.V. Trevisan, An overview of heavy oil properties and its recovery and transportation methods, *Braz. J. Chem. Eng.* 31 (2014) 571-590.

[3] P.Y. Wang, J. Wang, S.Q. Zheng, Y.M. Qi, M.X. Xiong, Y.J. Zheng, Effect of H₂S/CO₂, partial pressure ratio on the tensile properties of X80 pipeline steel, *Int. J. Hydrogen Energ.* 40 (2015) 11925-11930.

[4] A. Vairavamurthy, K. Mopper, Geochemical formation of organosulphur compounds (thiols) by addition of H₂S to sedimentary organic matter, *Nature* 329 (1987) 623-625.

[5] S.Q. Zheng, C.Y. Li, Y.M. Qi, L.Q. Chen, C.F. Chen, Mechanism of (Mg, Al, Ca)-oxide inclusion-induced pitting corrosion in 316L stainless steel exposed to sulphur environments containing chloride ion, *Corros. Sci.* 67 (2013) 20-31.

[6] F. Pessu, R. Barker, A. Neville, Pitting and uniform corrosion of X65 carbon steel in sour corrosion environments: the influence of CO₂, H₂S, and temperature, *Corrosion* 73 (2017) 1168-1183.

[7] M.A. Mohtadi-Bonab, J.A. Szpunar, R. Basu, M. Eskandari, The mechanism of failure by hydrogen induced cracking in an acidic environment for API 5L X70 pipeline steel, *Int. J. Hydrogen Energ.* 40 (2015) 1096-1107.

[8] F.Y. Kong, G.J. Hu, X. Li, Stress corrosion cracking of SPV50Q steel in H₂S-containing sour environment, *Advanced Materials Research. Trans. Tech. Publications* 314 (2011) 1087-1091.

[9] C.D. Wang, M.L. Yan, X.W. Zhao, Research progress of H₂S/CO₂ corrosion in oil and gas development, 20 (2005) 66.

[10] D.W. Shoesmith, P. Taylor, M.G. Bailey, B. Ikeda, Electrochemical behaviour of iron in alkaline sulphide solutions, *Electrochim. Acta* 23 (1978) 903-916.

[11] B.G. Pound, G.A. Wright, R.M. Sharp, The anodic behavior of iron in hydrogen sulfide solutions, *Corrosion* 45 (1989) 386-392.

[12] S.Q. Zheng, C.S. Zhou, X.Y. Chen, L. Zhang, J.Y. Zheng, Y.Z. Zhao, Dependence of the abnormal protective property on the corrosion product film formed on H₂S-adjacent API-X52 pipeline steel, *Int. J. Hydrogen Energ.* 39 (2014) 13919-13925.

[13] Y.M. Qi, H.Y. Luo, S.Q. Zheng, C.F. Chen, Z.G. Lv, M.X. Xiong, Effect of H₂S partial pressure on the tensile properties of A350LF2 steel in the absence and presence of pre-immersion, *Mat. Sci. Eng. A* 609 (2014) 161-167.

[14] Y.M. Qi, H.Y. Luo, S.Q. Zheng, C.F. Chen, D.N. Wang, Effect of immersion time on the hydrogen content and tensile properties of A350LF2 steel exposed to

hydrogen sulphide environments, *Corros. Sci.* 69 (2013) 164-174.

[15] C.S. Zhou, S.Q. Zheng, C.F. Chen, G.W. Lu, The effect of the partial pressure of H₂S on the permeation of hydrogen in low carbon pipeline steel, *Corros. Sci.* 67 (2013) 184-192.

[16] H.Y. Ma, X.L. Cheng, G.Q. Li, S.H. Chen, Z.L. Quan, S.Y. Zhao, L. Niu, The influence of hydrogen sulfide on corrosion of iron under different conditions, *Corros. Sci.* 42 (2000) 1669-1683.

[17] S.Q. Zheng, L.W. Liu, C.S. Zhou, L.Q. Chen, C.F. Chen, Effects of H₂S-containing corrosive media on the crystal structures of corrosion product films formed on L360NCS, *Int. J. Electrochem. Sci.* 8 (2013) 1434-1442.

[18] D. Rickard, J.W. Morse, Acid volatile sulfide (AVS), *Mar. Chem.* 97 (2005) 141-197.

[19] F.H. Meyer, O.L. Riggs, R.L. Mcglasson, J.D. Sudbury, Corrosion products of mild steel in hydrogen sulfide environments, *Corrosion*, 14 (1958) 109-115.

[20] S.N. Smith, Current understanding of corrosion mechanisms due to H₂S in oil and gas production environments, *NACE Corrosion* 2015.

[21] A. Traidia, M. Alfano, G. Lubineau, S. Duval, A. Sherik, An effective finite element model for the prediction of hydrogen induced cracking in steel pipelines, *Int. J. Hydrogen Energ.* 37 (2012) 16214-16230.

[22] S. Gao, P. Jin, B. Brown, D. Young, S. Nešić, M. Singer, Effect of high temperature on the aqueous H₂S corrosion of mild steel, *Corrosion* 2017.

[23] A. Kahyarian, A. Schumaker, B. Brown, S. Nešić, Acidic corrosion of mild steel in the presence of acetic acid: mechanism and prediction, *Electrochim. Acta* 258 (2017) 639-652.

[24] G.A. Zhang, Y. Zeng, X.P. Guo, F. Jiang, D.Y. Shi, Z.Y. Chen, Electrochemical corrosion behavior of carbon steel under dynamic high pressure H₂S/CO₂ environment, *Corros. Sci.* 65 (2012) 37-47.

[25] O.M. Suleimenov, R.E. Krupp. Solubility of hydrogen sulfide in pure water and in NaCl solutions, from 20 to 320 °C and at saturation pressures, *Geochim. Cosmochim. Ac.* 58 (1994) 2433-2444.

[26] O.M. Suleimenov, T.M. Seward, A spectrophotometric study of hydrogen sulphide ionisation in aqueous solutions to 350 °C, *Geochim. Cosmochim. Ac.* 61 (1997) 5187-5198.

[27] Y.K. Kharaka, W.D. Gunter, P.K. Aggarwal, E.H. Perkins, J.D. DeBraal, SOLMINEQ. 88: A computer program for geochemical modeling of water-rock interactions, US geological survey water-resources investigation report 88 (1988) 4277.

[28] X.L. Cheng, H.Y. Ma, J.P. Zhang, X. Chen, S.H. Chen, H.Q. Yang, Corrosion of iron in acid solutions with hydrogen sulfide, *Corrosion* 54 (1998) 369-376.

[29] M.A. Lucio-Garcia, J.G. Gonzalez-Rodriguez, M. Casales, L. Martinez, J.G. Chacon-Nava, M.A. Neri-Flores, A. Martinez-Villafañe, Effect of heat treatment on H₂S corrosion of a micro-alloyed C-Mn steel, *Corros. Sci.* 51 (2009) 2380-2386.

[30] W. Sun, Kinetics of iron carbonate and iron sulfide scale formation in CO₂/H₂S corrosion, PhD Thesis, Ohio University, 2006.

[31] P. Marcus, E. Protopopoff, Potential-pH diagrams for adsorbed species. Application to sulfur adsorbed on iron in water at 25 °C and 300 °C, *J. Electrochem. Soc.* 137 (1990) 2709-2712.

[32] Y. Zheng, B. Brown, S. Nešić, Electrochemical study and modeling of H₂S corrosion of mild steel, *Corrosion*, 70 (2013) 351-365.

[33] L.G. Benning, R.T. Wilkin, H.L. Barnes, Reaction pathways in the Fe-S system below 100 °C, *Chem. Geol.* 167 (2000) 25-51.

[34] D. Rickard, Kinetics of FeS precipitation: Part 1. Competing reaction mechanisms, *Geochim. Cosmochim. Ac.* 59 (1995) 4367-4379.

[35] N.G. Harmandas, P.G. Koutsoukos, The formation of iron (II) sulfides in aqueous solutions, *J. Cryst. Growth* 167 (1996) 719-724.

[36] W. Sun, S. Nešić, Kinetics of corrosion layer formation: part 1-iron carbonate layers in carbon dioxide corrosion, *Corrosion* 64 (2008) 334-346.

[37] H. Ma, X. Cheng, S. Chen. C. Wang, J. Zhang, H. Yang, An ac impedance study of the anodic dissolution of iron in sulfuric acid solutions containing hydrogen sulfide, *J. Electroanal. Chem.* 451 (1998) 11-17.

[38] M. Elboudjaini, R.W. Revie, Metallurgical factors in stress corrosion

cracking (SCC) and hydrogen-induced cracking (HIC), *J. Solid. State. Electr.* 13 (2009) 1091-1099.

[39] K.A. Esaklul, *Hydrogen damage, Trends in Oil and Gas Corrosion Research and Technologies 2017.*

[40] S.Q. Zheng, C.F. Chen, L.Q. Chen, Corrosion characteristics of 2205 duplex Stainless steel in high temperature and high pressure environment containing H₂S/CO₂, *Advanced Materials Research. Trans. Tech. Publications* 236 (2012) 95-98.

[41] M. Alizadeh, S. Bordbar, The influence of microstructure on the protective properties of the corrosion product layer generated on the welded API X70 steel in chloride solution, *Corros. Sci.* 70 (2013) 170-179.

[42] P.P. Bai, S.Q. Zheng, C.F. Chen, Electrochemical characteristics of the early corrosion stages of API X52 steel exposed to H₂S environments, *Mater. Chem. Phys.* 149 (2015) 295-301.

[43] J. Zhou, P.P. Bai, T.Q. Wang, S.Q. Zheng, Effect of ferrous ion on the corrosion behaviour of 410 stainless steel in wet H₂S environment, *Materials Science Forum. Trans Tech Publications Ltd.* 850 (2016) 1016-1021.

[44] J. Kvarekvål, J. Moloney, *Sour corrosion, Trends in Oil and Gas Corrosion Research and Technologies 2017.*

[45] D. Rickard, G.W. Luther, Chemistry of iron sulfides, *Chem. Rev.* 107 (2007) 514-562.

[46] J.B. Sardisco, W.B. Wright, E.C. Greco, Corrosion of iron in on H₂S-CO₂-H₂O system: corrosion film properties on pure iron, *Corrosion* 19 (1963) 354-359.

[47] S.N. Smith, M.W. Joosten, Corrosion of carbon steel by H₂S in CO₂ containing oilfield environments-10 Year update, *NACE International 2015.*

[48] D.T. Rickard, Kinetics of FeS precipitation: Part 1. Competing reaction mechanisms, *Geochim. Cosmochim. Ac.* 59 (1995) 4367-4379.

[49] H.Y. Jeong, J.H. Lee, K.F. Hayes, Characterization of synthetic nanocrystalline mackinawite: crystal structure, particle size, and specific surface area, *Geochim. Cosmochim. Ac.* 72 (2008) 493-505.

[50] P.P. Bai, H. Zhao, S.Q. Zheng, C.F. Chen, Initiation and developmental

stages of steel corrosion in wet H₂S environments, *Corros. Sci.* 93 (2015) 109-119.

[51] P.P. Bai, S.Q. Zheng, H. Zhao, Y. Ding, J. Wu, C.F. Chen, Investigations of the diverse corrosion products on steel in a hydrogen sulfide environment, *Corros. Sci.* 87 (2014) 397-406.

[52] D.W. Shoesmith, P. Taylor, M.G. Bailey, D.G. Owen, The formation of ferrous monosulfide polymorphs during the corrosion of iron by aqueous hydrogen sulfide at 21 °C, *J. Electrochem. Soc.* 127 (1980) 1007-1015.

[53] S.N. Smith, B.N. Brown, W.N. Sun, Corrosion at higher H₂S concentrations and moderate temperatures, *Corrosion* 2011.

[54] S.Q. Zheng, C.Y. Li, C.F. Chen, Effect of temperature on the corrosion behaviours of L360QCS in the environments containing elemental sulphur and H₂S/CO₂, *Металлофизика и новейшие технологии* 34 (2012) 57-63.

[55] Y.M. Qi, H.Y. Luo, S.Q. Zheng, C.F. Chen, Z.G. Lv, M.X. Xiong, Effect of temperature on the corrosion behavior of carbon steel in hydrogen sulphide environments, *Int. J. Electrochem. Sc.* 9 (2014) 2101-2112.

[56] E. Sosa, R. Cabrera-Sierra, M.E. Rincén, M.T. Oropeza, I. González, Evolution of non-stoichiometric iron sulfide film formed by Electrochemical oxidation of carbon steel in alkaline sour environment, *Electrochim. Acta* 47 (2002) 1197-1208.

[57] J. Amri, J. Kvarekvål, B. Malki, Simulation of solid-state growth of iron sulfides in sour corrosion conditions, *NACE Corrosion* 12 (2011) 246-248.

[58] F.W. Herbert, Mechanisms governing the growth, reactivity and stability of iron sulfides, Massachusetts Institute of Technology 2015.

[59] J. Ning, Y.G. Zheng, D. Young, B. Brown, S. Nešić, Thermodynamic study of hydrogen sulfide corrosion of mild steel, *Corrosion* 70 (2013) 375-389.

[60] J. Ning, Y.G. Zheng, B. Brown, D. Young, S. Nešić, A thermodynamic model for the prediction of mild steel corrosion products in an aqueous hydrogen sulfide environment, *Corrosion* 71 (2015) 945-960.

[61] L. Zhang, H.X. Li, F.X. Shi, J.W. Yang, L.H. Hu, M.X. Lu, Environmental boundary and formation mechanism of different types of H₂S corrosion products on pipeline steel, *Int. J. Min. Met. Mater.* 24 (2017) 401-409.

[62] X.L. Wen, Y.X. Liang, P.P. Bai, B.W. Luo, T. Fang, L. Yue, T. An, W.Y. Song, S.Q. Zheng, First-principles calculations of the structural, elastic and thermodynamic properties of mackinawite (FeS) and pyrite (FeS₂), *Physica. B* 525 (2017) 119-126.

[63] H.Y. Jeong, J.H. Lee, K.F. Hayes, Characterization of synthetic nanocrystalline mackinawite: crystal structure, particle size, and specific surface area, *Geochim. Cosmochim. Ac.* 72 (2008) 493-505.

[64] L.Q. Chen, J. Zhou, Y.X. Chen, P.P. Bai, J. Wu, S.Q. Zheng, The dependence of electrochemical behaviors on the corrosion products of L360NCS steel exposed to wet H₂S environments, *Int. J. Electrochem. Sc.* 11 (2016) 3987-3999.

[65] H. Ohfuji, D. Rickard, High resolution transmission electron microscopic study of synthetic nanocrystalline mackinawite, *Earth Planet. Sc. Let.* 241 (2006) 227-233.

[66] S. Boursiquot, M. Mullet, M. Abdelmoula, J.M. Génin, J.J. Ehrhardt, The dry oxidation of tetragonal FeS_{1-x} mackinawite, *Phys. Chem. Miner.* 28 (2001) 600-611.

[67] D. Rickard, A. Griffith, A. Oldroyd, I.B. Butler, E. Lopez-Capel, D.A.C. Manning, D.C. Apperley, The composition of nanoparticulate mackinawite, tetragonal iron (II) monosulfide, *Chem. Geol.* 235 (2006) 286-298.

[68] G. Genchev, A. Erbe, Raman spectroscopy of mackinawite FeS in anodic iron sulfide corrosion products, *J. Electrochem. Soc.* 163 (1016) 333-338.

[69] M.R. De, Cubic FeS, a metastable iron sulfide, *Science* 170 (1970) 1191-1192.

[70] S. Takeno, H. Zoka, T. Niihara, Metastable cubic iron sulfide-with special reference to mackinawite, *Am. Mineral.* 55 (1970) 1639-1649.

[71] M. Pósfai, P.R. Buseck, D.A. Bazylinski, R.B. Frankei, Iron sulfides from magnetotactic bacteria: structure, composition, and phase transitions, *Am. Mineral.* 83 (1998) 1469-1481.

[72] A.J. Devey, Computer modelling studies of mackinawite, greigite and cubic FeS, PhD Thesis, UCL (University College London), 2010.

[73] J.B. Murowchick, H.L. Barnes, Formation of cubic FeS, *Am. Mineral.* 71 (1986) 1243-1246.

[74] G.W. Luther, S.M. Theberge, D.T. Rickard, Evidence for aqueous clusters as intermediates during zinc sulfide formation, *Geochim. Cosmochim.* 63 (1999) 3159-3169.

[75] A.V. Powell, P. Vaquero, K.S. Knight, L.C. Chapon, R.D. Sánchez, Structure and magnetism in synthetic pyrrhotite Fe_7S_8 : A powder neutron-diffraction study, *Phys. Rev. B* 70 (2004) 014415.

[76] M. Pósfai, T.G. Sharp, A. Kontny, Pyrrhotite varieties from the 9.1 km deep borehole of the KTB project, *Am. Mineral.* 85 (2000) 1406-1415.

[77] Q. Liu, J. Whittaker, R. Marsden, Mystery of SAGD casing gas corrosivity and corrosion mitigation strategy, NACE International 2015.

[78] R.A. Berner, Stability fields of iron minerals in anaerobic marine sediments, *J. Geol.* 72 (1964) 826-834.

[79] J.B. Sardisco, R.E. Pitts, Corrosion of iron in an H_2S - CO_2 - H_2O system mechanism of sulfide film formation and kinetics of corrosion reaction, *Corrosion* 21 (1965) 245-253.

[80] W.H. Thomason, Formation rates of protective iron sulfide films on mild steel in H_2S saturated brine as a function of temperature, *Corrosion* 78, Houston, TX, March 6-10, 1978.

[81] A.G. Wikjord, T.E. Rummery, F.E. Doern, D.G. Owen, Corrosion and deposition during the exposure of carbon steel to hydrogen sulphide-water solutions, *Corros. Sci.* 20 (1980) 651-671.

[82] T. Ramanarayanan, Scaling phenomena in high temperature aqueous and gaseous environments containing sulfur, 1989.

[83] H. Vedage, T.A. Ramanarayanan, J.D. Mumford, S.N. Smith, Electrochemical growth of iron sulfide films in H_2S -saturated chloride media, *Corrosion* 49 (1993) 114-121.

[84] J. Kvarekvål, R. Nyborg, H. Choi, Formation of multilayer iron sulfide films during high temperature $\text{CO}_2/\text{H}_2\text{S}$ corrosion of carbon steel, *Ann. Chir. Infant.* 3 (2003) 193-200.

[85] C.Q. Ren, D.X. Liu, Z.Q. Bai, T.H. Li, Corrosion behavior of oil tube steel

in simulant solution with hydrogen sulfide and carbon dioxide, *Mater. Chem. Phys.* 93 (2005) 305-309.

[86] H.J. Choi, D. Warnken, B.F.I. Al, et al., Field Corrosion assessment of L80 carbon steel downhole production tubing at khuff gas wells, NACE International 2006.

[87] E.H. Dehkordi, A.R. Tavakoli, The effect of time on the formation & growth of passive layer on carbon steel A516 GR. 70 in sour water, *Int. J. Iron. Steel Soc. Iran.* 4 (2007) 28-33.

[88] L. Zhang, J. Yang, J. Sun, L. Minxu, Effect of pressure on wet H₂S/CO₂ corrosion of pipeline steel, *J. Mater. Eng.* 32 (2009) 87-91.

[89] F.X. Shi, L. Zhang, J.W. Yang, M.X. Lu, J.H. Ding, H. Li, Polymorphous FeS corrosion products of pipeline steel under highly sour conditions, *Corros. Sci.* 102 (2016) 103-113.

[90] H.T. Evans, Lunar troilite: crystallography, *Science* 167 (1970) 621-623.

[91] R. Skála, I. Císařová, M. Drábek, Inversion twinning in troilite, *Am. Mineral.* 91 (2006) 917-921.

[92] H.E. King, C.T. Prewitt, High-pressure and high-temperature polymorphism of iron sulfide (FeS), *Acta. Crystallogr. B.* 38 (1982) 1877-1887.

[93] H. Wang, I. Salveson, A review on the mineral chemistry of the non-stoichiometric iron sulphide, Fe_{1-x}S (0 ≤ x ≤ 0.125): polymorphs, phase relations and transitions, electronic and magnetic structures, *Phase Transit.* 78 (2005) 547-567.

[94] L.A. Taylor, H.K. Mao, A high-pressure polymorph of troilite, FeS, *Science* 170 (1970) 850-851.

[95] M. Singer, A. Camacho, B. Brown, S. Nešić, Sour top-of-the-line corrosion in the presence of acetic acid, *Corrosion* 67 (2011) 085003-1-085003-16.

[96] B.J. Skinner, Greigite, the thio-spinel of iron; a new mineral, *Am. Mineral.* 49 (1964) 543-555.

[97] S. Mann, N.H.C. Sparks, R.B. Frankel, D.A. Bazylinski, H.W. Jannasch, Biomineralization of ferrimagnetic greigite (Fe₃S₄) and iron pyrite (FeS₂) in a magnetotactic bacterium, *Nature* 343 (1990) 258-261.

[98] C.T. Lefèvre, N. Menguy, F. Abreu, U. Lins, M. Pósfai, T. Prozorov, D.

Pignol, R.B. Frankel, D.A. Bazylinski, A cultured greigite-producing magnetotactic bacterium in a novel group of sulfate-reducing bacteria, *Science* 334 (2011) 1720-1723.

[99] A.P. Roberts, Magnetic properties of sedimentary greigite (Fe_3S_4), *Earth Planet. Sc. Let.* 134 (1995) 227-236.

[100] D.A. Kitchaev, G. Ceder, Evaluating structure selection in the hydrothermal growth of FeS_2 pyrite and marcasite, *Nat. Commun.* 7 (2016) 13799.

[101] I.B. Butler, D. Rickard, Framboidal pyrite formation via the oxidation of iron (II) monosulfide by hydrogen sulphide, *Geochim. Cosmochim.* 64 (2000) 2665-2672.

[102] D.W. Shoesmith, T.E. Rummery, M.G. Bailey, D.G. Owen, Electrocrystallization of pyrite and marcasite on stainless steel surfaces, *J. Electrochem. Soc.* 126 (1979) 911-919.

[103] K. Kusaba, W. Utsumi, M. Yamakata, O. Shimomura, Y. Syono, Second-order phase transition of FeS under high pressure and temperature, *J. Phys. Chem. Solids* 61 (2000) 1483-1487.

[104] Y. Liu, Iron sulfide precipitation kinetics, solubility, phase transformation, and corrosion versus temperature and ionic strength, PhD Thesis, Rice University, 2017.

[105] D.C. Johnson, D.R. Dean, A.D. Smith, M.K. Johnson, Structure, function, and formation of biological iron-sulfur clusters, *Annu. Rev. Biochem.* 74 (2005) 247-281.

[106] P.V. Vanitha, P. O'Brien, Phase control in the synthesis of magnetic iron sulfide nanocrystals from a cubane-type Fe-S cluster, *J. Am. Chem. Soc.* 130 (2008) 17256-17257.

[107] D.R. Cummins, H.B. Russell, J.B. Jasinski, M. Menon, M.K. Sunkara, Iron sulfide (FeS) nanotubes using sulfurization of hematite nanowires, *Nano Lett.* 13 (2013) 2423-2430.

[108] J. Wu, Y.X. Liang, P.P. Bai, S.Q. Zheng, L.Q. Chen, Microwave-assisted synthesis of pyrite FeS_2 microspheres with strong absorption performance, *RSC Adv.* 5 (2015) 65575-65582.

[109] A.R. Lennie, S.A.T. Redfern, P.E. Champness, C.P. Stoddart, P.F. Schofield,

D.J. Vaughan, An in situ X-ray powder diffraction and transmission electron microscope study, *Am. Mineral.* 82 (1997) 302-309.

[110] S.K. Bhargava, A. Garg, N.D. Subasinghe, In situ, high-temperature phase transformation studies on pyrite, *Fuel* 88 (2009) 988-993.

[111] S. Ono, A.R. Oganov, J.P. Brodholt, L. Vočadlo, I.G. Wood, A. Lyakhov, C.W. Glass, A.S. Côté, G.D. Price, High-pressure phase transformations of FeS: novel phases at conditions of planetary cores, *Earth Planet. Sc. Let.* 272 (2008) 481-487.

[112] S.N. Smith, E.J. Wright, Prediction of minimum H₂S levels required for slightly sour corrosion, *NACE Corrosion* 1994.

[113] S.N. Smith, M.W. Joosten, Corrosion of carbon steel by H₂S in CO₂ containing oilfield environments, *NACE International* 2006.

[114] W. Sun, S. Papavinasam, S. Nešić, Kinetics of iron sulfide and mixed iron sulfide/carbonate scale precipitation in CO₂/H₂S corrosion, *Corrosion* 2006.

[115] C.S. Zhou, X.Y. Chen, Z. Wang, S.Q. Zheng, X. Li, L. Zhang, Effects of environmental conditions on hydrogen permeation of X52 pipeline steel exposed to high H₂S-containing solutions, *Corros. Sci.* 89 (2014) 30-37.

[116] M. Liu, J. Wang, W. Ke, Corrosion behaviour of X52 pipeline steel in high H₂S concentration solutions at temperatures ranging from 25 °C to 140 °C, *Brit. Corros. J.* 48 (2013) 380-387.

[117] P.P. Bai, S.Q. Zheng, C.F. Chen, H. Zhao, Investigation of the iron-sulfide phase transformation in nanoscale, *Cryst. Growth Des.* 14 (2014) 4295-4302.

[118] Y. Li, R.A. van Santen, T. Weber, High-temperature FeS-FeS₂ solid-state transitions: Reactions of solid mackinawite with gaseous H₂S, *J. Solid State Chem.* 181 (2008) 3151-3162.

[119] S.N. Esmaeely, S. Nešić, Reduction reactions on iron sulfides in aqueous acidic solutions, *J. Electrochem. Soc.* 164 (2017) 664-670.

[120] P. Taylor, T.E. Rummery, D.G. Owen, Reactions of iron monosulfide solids with aqueous hydrogen sulfide up to 160 °C, *J. inorg. Nucl. Chem.* 41 (1979) 1683-1687.

[121] S. Smith, E. Wright, Prediction of corrosion in slightly sour environments,

NACE Corrosion 2002.

[122] J. Ning, Y. Zheng, B. Brown, D. Young, S. Nešić, Construction and verification of Pourbaix diagrams for hydrogen sulfide corrosion of mild steel, NACE International 2015.

[123] E. Wallaert, T. Depover, I. Graeve, K. Verbeken, FeS corrosion products formation and hydrogen uptake in a sour environment for quenched & tempered steel, *Metals* 8 (2018) 62-75.

[124] B. Sherar, I. Power, P. Keech, S. Mitlin, G. Southam, D. Shoesmith, Characterizing the effect of carbon steel exposure in sulfide containing solutions to microbially induced corrosion, *Corros. Sci.* 53 (2011) 955-960.

[125] E. Miranda, M. Bethencourt, F. Botana, M. Cano, J. Sánchez-Amaya, A. Corzo, J. Lomas, M. Fardeau, B. Ollivier, Biocorrosion of carbon steel alloys by an hydrogenotrophic sulfate-reducing bacterium *Desulfovibrio capillatus*, isolated from a Mexican oil field separator, *Corros. Sci.* 48 (2006) 2417-2431.

[126] M. Gayosso, G. Olivares, N. Ordaz, C. Ramirez, C. Ramirez, A. Viveros, Microbial consortium influence upon steel corrosion rate, using polarisation resistance and electrochemical noise techniques, *Electrochim. Acta* 49 (2004) 4295-4301.

[127] M. C. Fatah, M. C. Ismail, B. A. Wahjoedi, Effects of sulphide ion on corrosion behaviour of X52 steel in simulated solution containing metabolic products species: a study pertaining to microbiologically influenced corrosion (MIC), *Brit. Corros. J.* 48 (2013) 211-220.

[128] R. Edyvean, Hydrogen sulphide - A corrosive metabolite, *Int. Biodeter.* 27 (1991) 109-120.

[129] M. Liu, J. Wang, W. Ke, Effect of temperature and H₂S concentration on corrosion of X52 pipeline steel in acidic solutions, *Mater. Sci. Forum.* 744 (2013) 589-596.

[130] M. Liu, J. Wang, W. Ke, E. Han, Corrosion behavior of X52 anti-H₂S pipeline steel exposed to high H₂S concentration solutions at 90 °C, *J. Mater. Sci. Technol.* 30 (2014) 504-510.

[131] D. Li, W. Hao, Y. Liu, L. Zhang, M. Lu, J. Wang, Effect of H₂S content on

corrosion behavior and hydrogen permeation of pipeline steel, NACE International 2014.

[132] Y. Zheng, J. Ning, D. Young, B. Brown, D. Young, S. Nešić, Mechanistic study of the effect of iron sulfide layers on hydrogen sulfide corrosion of carbon steel, *Corrosion*. 2015.

[133] Z. Wang, M.L. Liu, M.X. Lu, L. Zhang, J.Y. Sun, Z.R. Zhang, X. Tang, The effect of temperature on the hydrogen permeation of pipeline steel in wet hydrogen sulfide environments, *Int. J. Electrochem. Sci*, 13 (2018) 915-924.

[134] W. Zhao, Y. Zou, K.J. Matsuda, Z.D. Zou, Characterization of the effect of hydrogen sulfide on the corrosion of X80 pipeline steel in saline solution, *Corros. Sci.* 102 (2016) 455-468.

[135] S. Navabzadeh, G.M. Bota, B. Brown, S. Nešić, Influence of pyrrhotite on the corrosion of mild steel, *Corrosion*, 2017.

[136] A. Krishnamoorthy, Modeling of mechanisms affecting the growth and breakdown of iron sulfide films, Massachusetts Institute of Technology 2016.

[137] T. Omura, T. Kobayashi, M. Ueda, SSC resistance of high strength low alloy steel OCTG in high pressure H₂S environments, NACE International 2009.

[138] A. Krishnamoorthy, M.A. Dinh, B. Yildiz, Hydrogen weakens interlayer bonding in layered transition metal sulfide Fe_{1+x}S, *J. Mater. Chem. A*. 5 (2017) 5030-5035.

[139] Y. Jing, X. Tan, Z. Zhou, P.W. Shen, Tuning electronic and optical properties of MoS₂ monolayer via molecular charge transfer, *J. Mater. Chem. A*. 2 (2014) 16892-16897.

[140] S. Standlee, K.D. Efird, D. Spiller, Under deposit corrosion from iron sulfide, NACE International 2011.

[141] R.A. King, J.D.A. Miller, J.S. Smith, Corrosion of mild steel by iron sulphides, *Brit. Corros. J.* 8 (1973) 137-141.

[142] Y. Zhang, J. Moloney, Corrosion monitoring under iron sulfide deposit: Testing method development, NACE International 2014.

[143] Y. Zhang, J. Moloney, Electrochemical corrosion rate measurement under

iron sulfide deposit: Testing method development, *Corrosion*, 72 (2015) 704-715.

[144] H. Sun, H. Fang, J. Davis, et al., Investigation of effects of iron sulfide on corrosion and inhibition of carbon steel in H₂S containing conditions, *NACE Corrosion* 33 (2012) 777-795.

[145] P.P. Bai, Y.X. Liang, S.Q. Zheng, C.F. Chen, Effect of amorphous FeS semiconductor on the corrosion behavior of pipe steel in H₂S-containing environments, *Ind. Eng. Chem. Res.* 55 (2016) 10932-10940.

Figure and Table Captions:

Figure 1: H₂S corrosion mechanism and hydrogen permeation processes. Adapted with permission [21]. Copyright 2012, Elsevier Publishing.

Figure 2: Various forms of hydrogen damage in carbon steel. Adapted with permission [39]. Copyright 2017, Elsevier Publishing.

Figure 3: Topography and surface potential images of a polished steel substrate before exposure to H₂S. (a) Morphology at low magnification; (b) surface potential distribution of the same area as (a); (c) Atomic force microscopy image of the sample surface after exposure to H₂S-H₂O vapour at 50 °C for 10 s. Reproduced with permission [50]. Copyright 2015, Elsevier Publishing.

Figure 4: SEM and 3D models of the morphology of the different corrosion products. (a) SEM image and (b) 3D model of the flake-shaped mackinawite obtained after 6 h; (c) SEM image and (d) 3D model of the octahedral cubic FeS obtained after 12 h; (e) SEM image and (f) 3D model of the framboidal pyrite obtained after 48 h; SEM micrograph of (g) beam-shaped troilite obtained after 18 h and (i) hexagonal wire-shaped troilite obtained after 21 h; (h) 3D model corresponding to (g) and (i). Adapted with permission [51]. Copyright 2014, Elsevier Publishing.

Figure 5: Pourbaix diagrams of the H₂S-H₂O-Fe system showing step changes in temperature up to 250 °C (T = 25 °C-250 °C, [H₂S]_{aq} = 9.4×10⁻³ M, [Fe²⁺] = 10 ppm, [Fe³⁺] = 10⁻⁶ M): (a) mackinawite/greigite; (b) pyrrhotite/pyrite. Pourbaix diagrams for the H₂S-H₂O-Fe system showing step changes in H₂S partial pressure (pH₂S = 100 ppm

- 10 bar, $T = 80\text{ }^{\circ}\text{C}$, $[\text{Fe}^{2+}] = 10\text{ ppm}$, $[\text{Fe}^{3+}] = 10^{-6}\text{ M}$): (c) mackinawite/greigite; (d) pyrrhotite/pyrite. Reproduced with permission [60]. Copyright 2015, Corrosion - Houston Tx- Publishing.

Figure 6: H_2S corrosion products at various temperatures and H_2S partial pressure. The closed symbols refer to experiment results verified by the model, and the open symbols refer to modelled data. Adapted with permission [61]. Copyright 2017, Springer Publishing.

Figure 7: (a) Unit cells of common pyrrhotite structures projected onto the (001) plane and compared to the NiAs unit cell. The grey dots represent Fe positions, and the numbers 1, 2, 3, and 4 mark four possible vacancy sites. In this case, vacant sites are illustrated by the black dots in position 2. Selected-area electron diffraction (SAED) patterns from (b) 1C crystals in $[0\bar{1}2]$, (c) 2C crystals in $[110]$, (d) 4C crystals in $[110]$, and (e) 5C crystals in $[010]$. Reproduced with permission [76]. Copyright 2000, Mineralogical Society of America Publishing.

Figure 8: Phase transitions of troilite with increasing temperature. Adapted with permission [93]. Copyright 2005, Taylor & Francis Publishing.

Figure 9: SEM image after sour top-of-the-line corrosion exposure (0.2 MPa CO_2 , 0.013 MPa H_2S , $T\ 70\text{ }^{\circ}\text{C}$, 3 weeks exposure). Adapted with permission [95]. Copyright 2011, NACE International Publishing.

Figure 10: Normalised intensities as a function of temperature for (a) air, (b) argon, and (c) CO_2 environments. Reproduced with permission [110]. Copyright 2009, Elsevier Publishing.

Figure 11: Phase diagram of troilite as a function of pressure. Adapted with permission [111]. Copyright 2008, Elsevier Publishing.

Figure 12: Transformation of cubic FeS into greigite. (A) Low-magnification TEM image of cubic FeS in transition at 21 h. The studied images were relocated inside the black boxes. (B) HRTEM image, (C) corresponding fast Fourier transform (FFT) pattern, and (D) SAED pattern of the cubic FeS in transition. (E) SAED patterns showing two sets of diffraction patterns attributed to the $[001]$ planes of cubic FeS and

greigite. Adapted with permission [117]. Copyright 2014, American Chemical Society (ACS) Publishing.

Figure 13: (a, b) XRD patterns and (c, d) XPS spectra of non-oxidized mackinawite after reaction with H₂S (a, c) at different temperatures for 3 h and (b, d) for different periods at 150 °C. M: mackinawite; P₁: Fe₉S₁₀; P₂: Fe₇S₈. Adapted with permission [118]. Copyright 2008, Elsevier Publishing.

Figure 14: Hydrogen permeation transients measured for 3 mm steel membranes exposed to test solutions of 5% NaCl and 1 MPa H₂S or 5% NaCl and 0.1 MPa H₂S. The arrows show the conditions of the corresponding SEM images of the specimen surface. Reproduced with permission [15]. Copyright 2013, Elsevier Publishing.

Figure 15: (a) Effect of molecular hydrogen and atom hydrogen interstitials on the ultimate strength and elastic modulus; (b) atomic H interstitials create dipolar attractive interactions among layers; (c) molecular H₂ interstitials induce steric repulsion between the layers. Reproduced with permission [138]. Copyright 2017, Royal Society of Chemistry (RSC) Publishing.

Figure 16: Corrosion vs. time curves for mild steel samples in the presence of various amounts of (a) mackinawite (Fe_{1+x}S), (b) greigite (Fe₃S₄), (c) smythite (Fe_gS₄), and (d) pyrite (FeS₂). Reproduced with permission [141]. Copyright 1973, Taylor & Francis Publishing. × 0.9 mmol sulphide; □ 1.8 mmol sulphide; ○ 2.7 mmol sulphide; △ 3.6 mmol sulphide; ● tris buffer alone

Figure 17: Polarization resistance and corrosion rate as functions of the potential scan rate in the presence of (a) 1 mm and (b) 5 mm iron sulphide deposits. Adapted with permission [143]. Copyright 2015, Corrosion -Houston Tx- Publishing.

Figure 1:

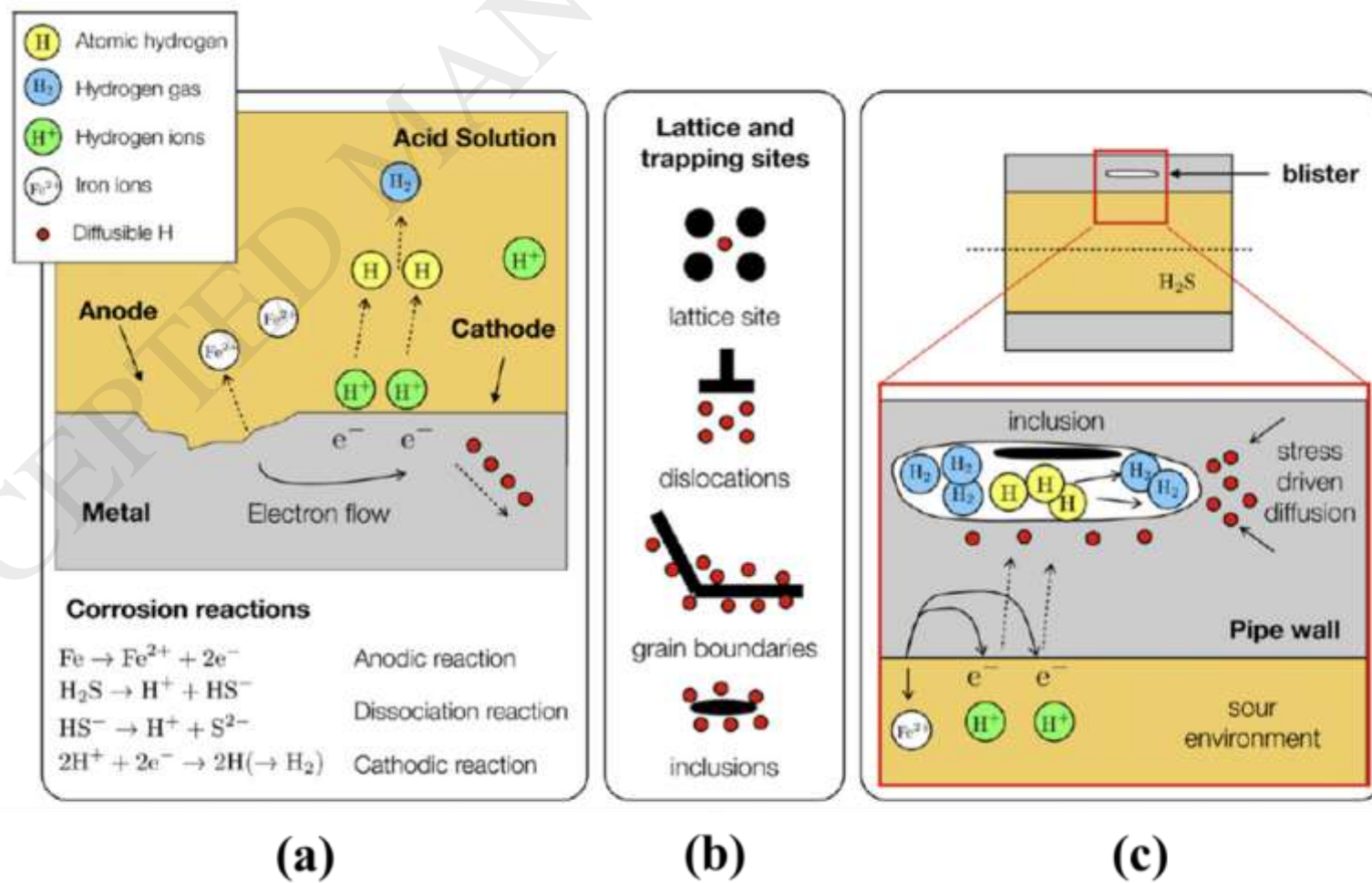


Figure 2:

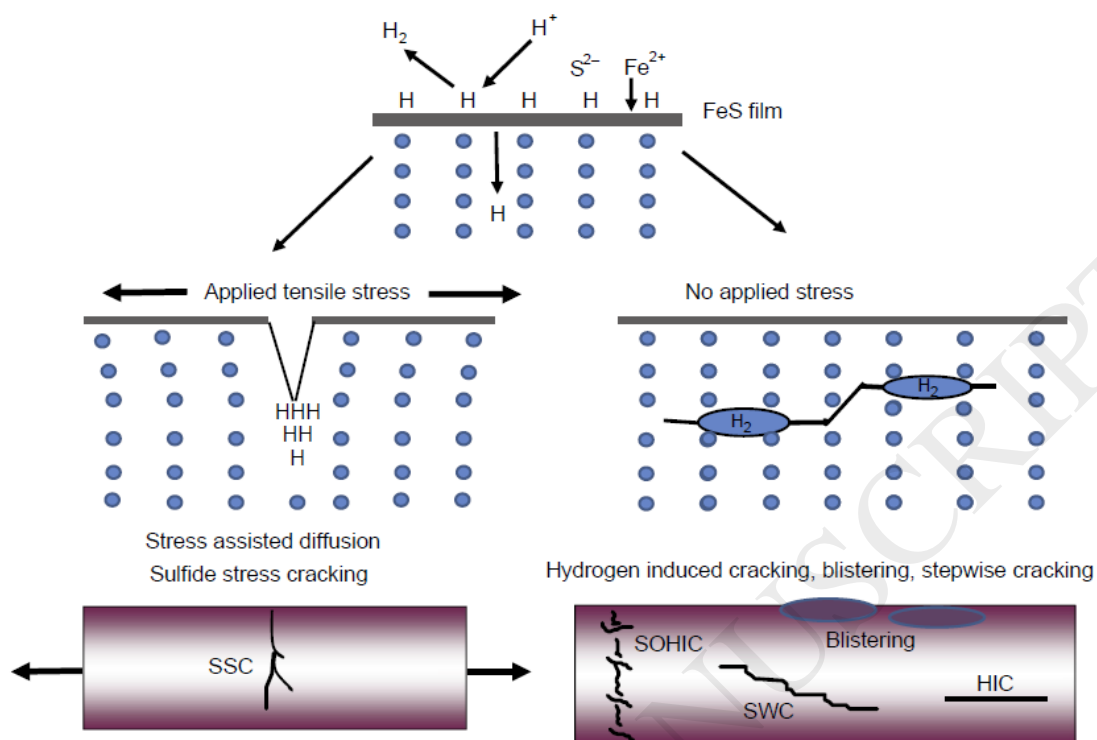


Figure 3:

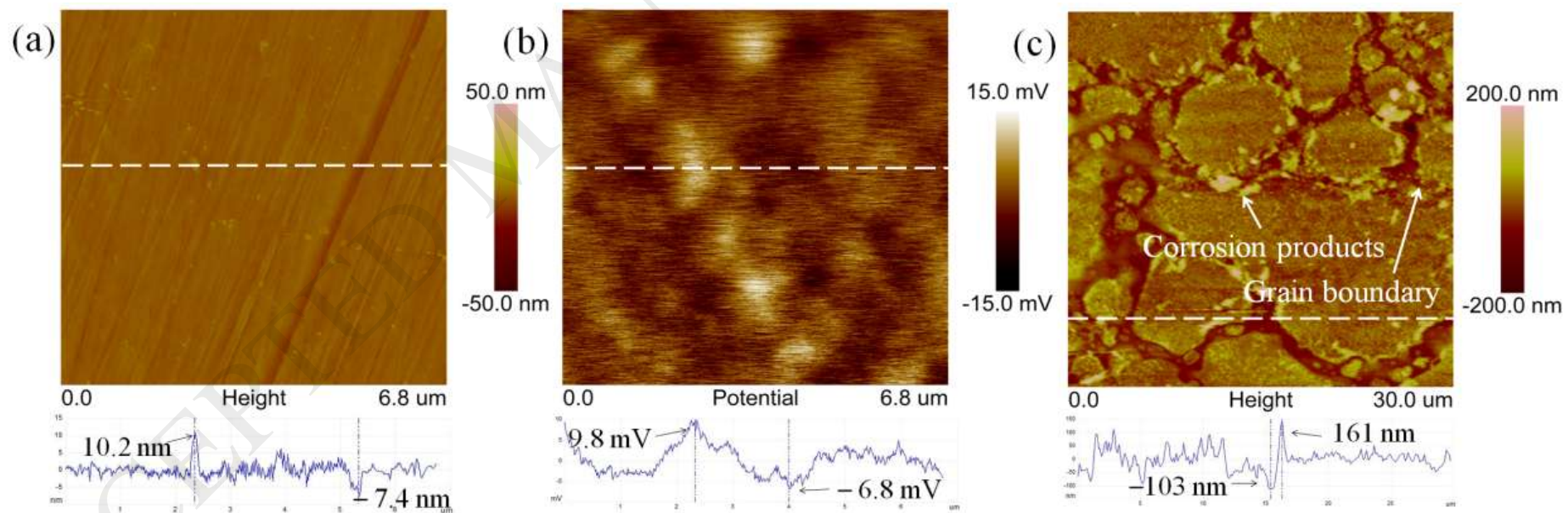


Figure 4:

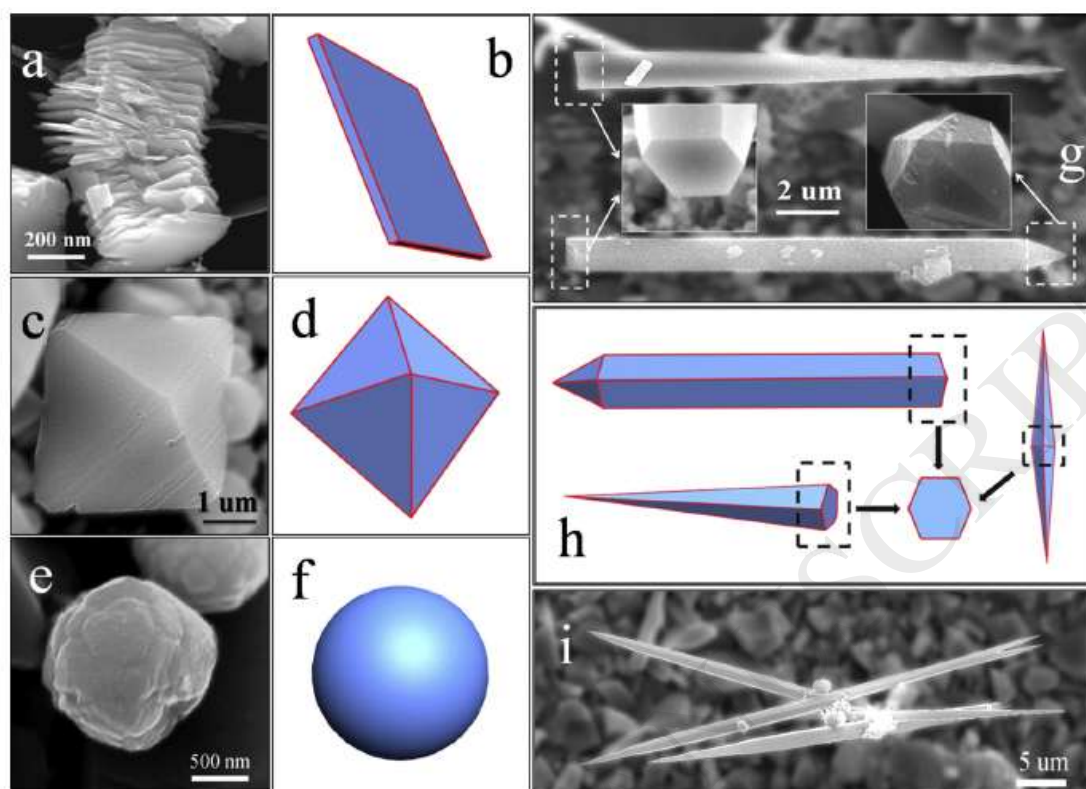


Figure 5:

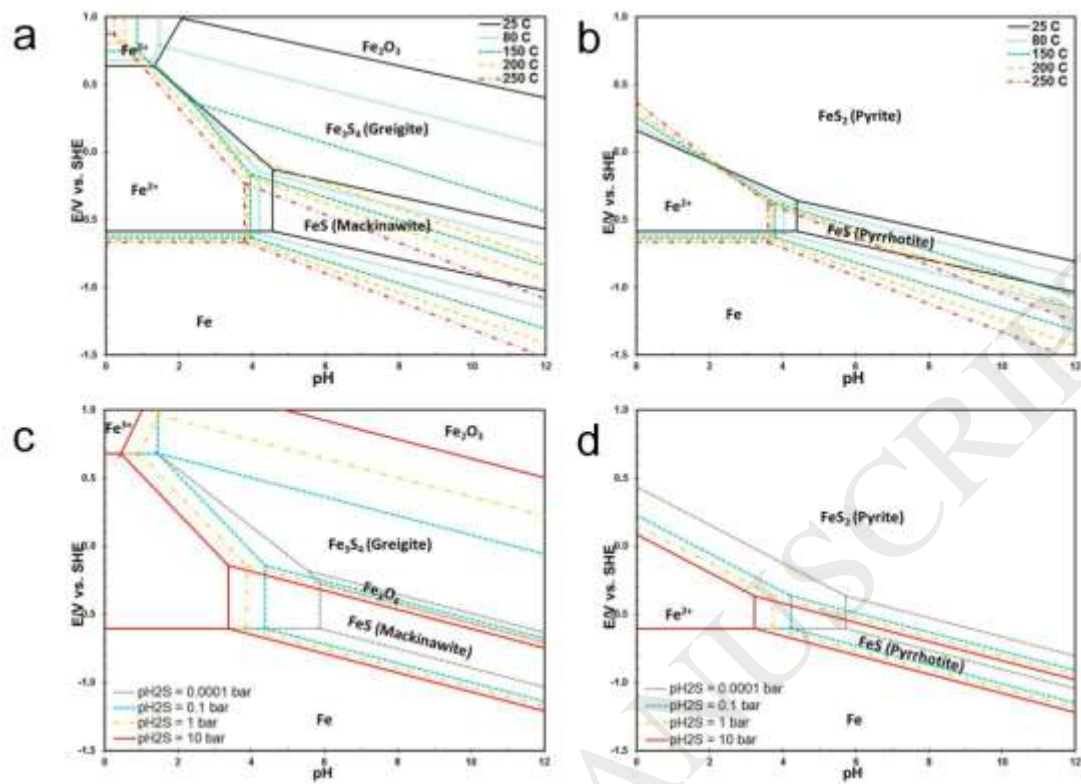


Figure 6:

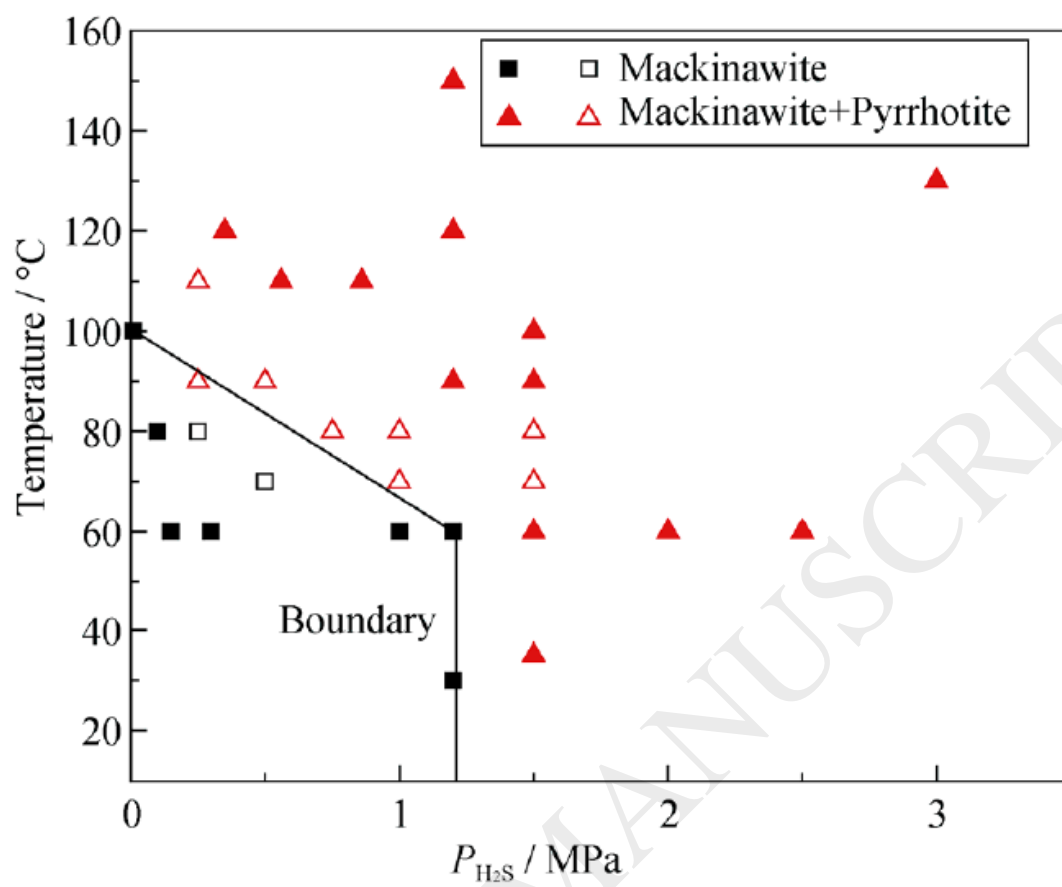


Figure 7:

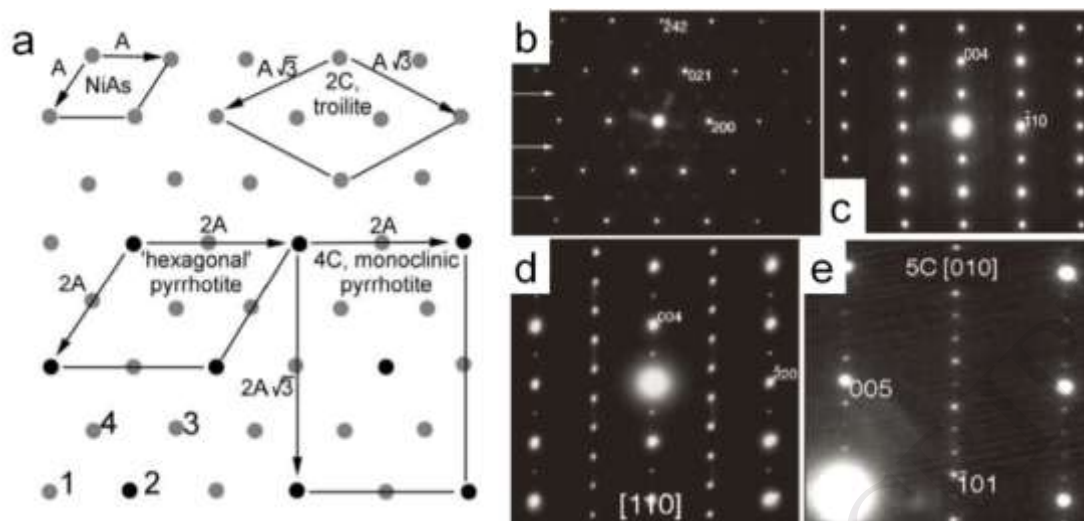


Figure 8:

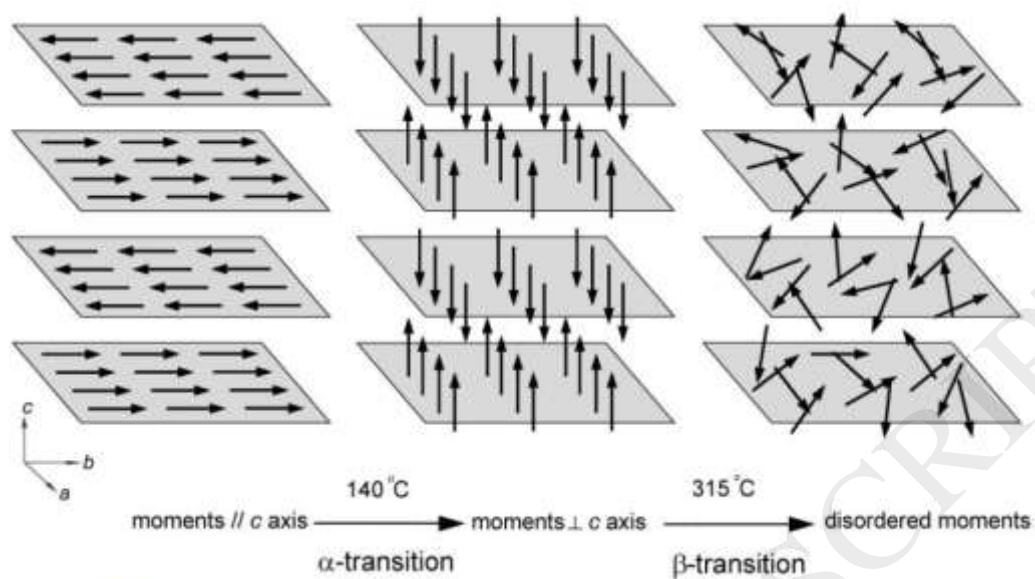


Figure 9:

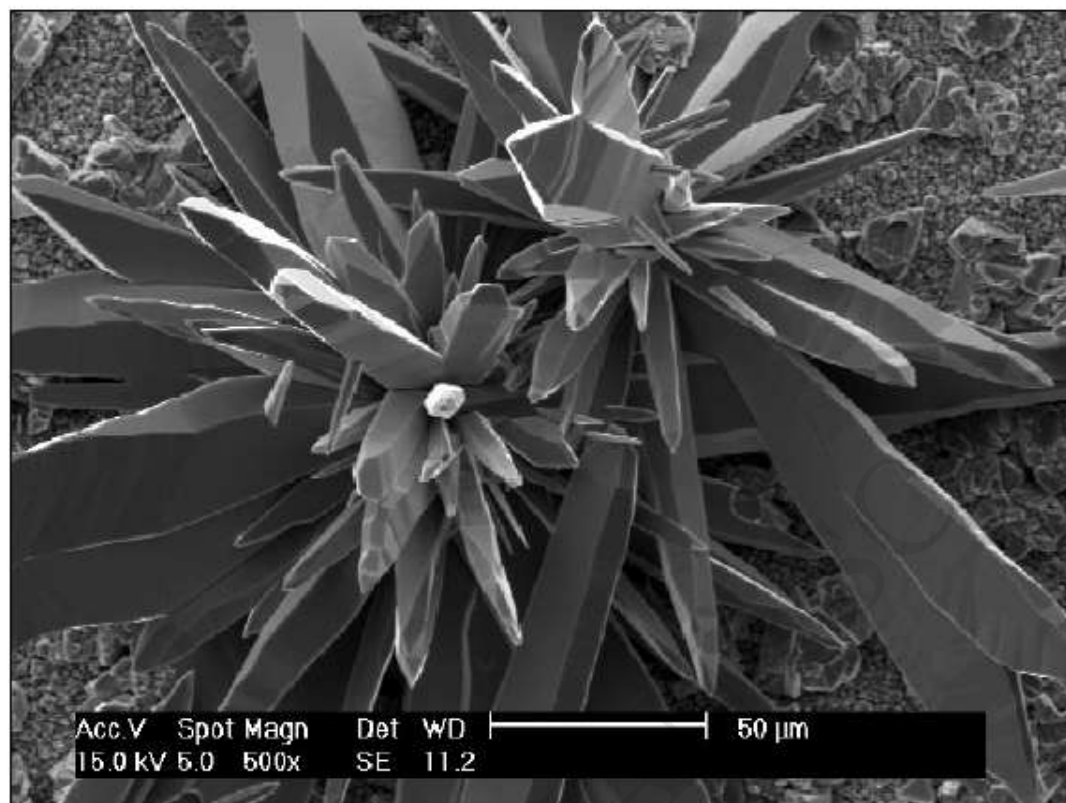


Figure 10:

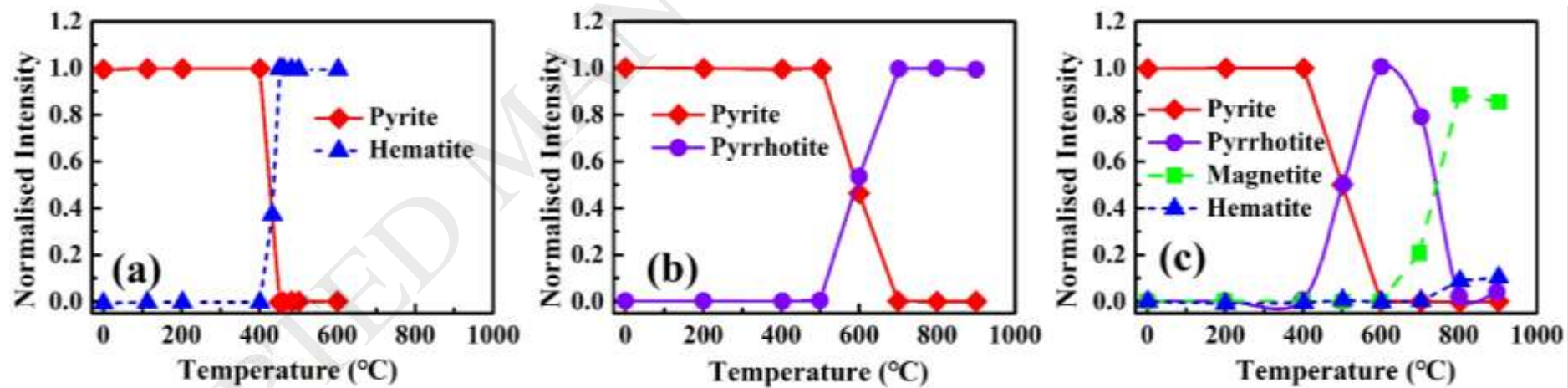


Figure 11:

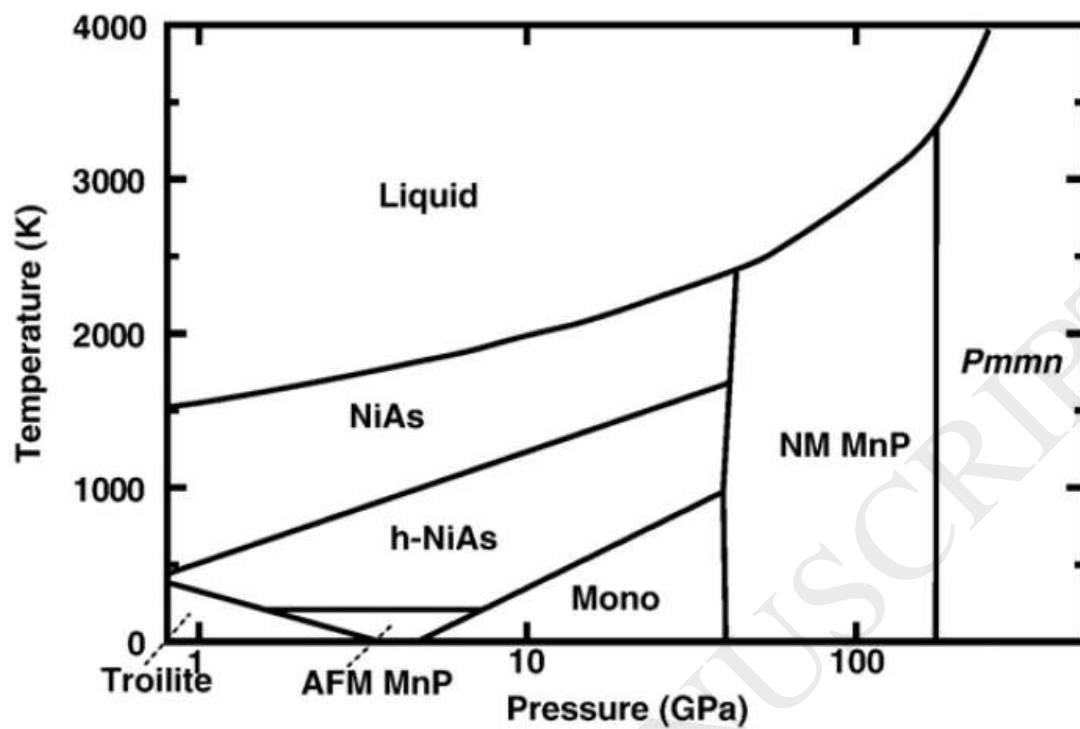


Figure 12:

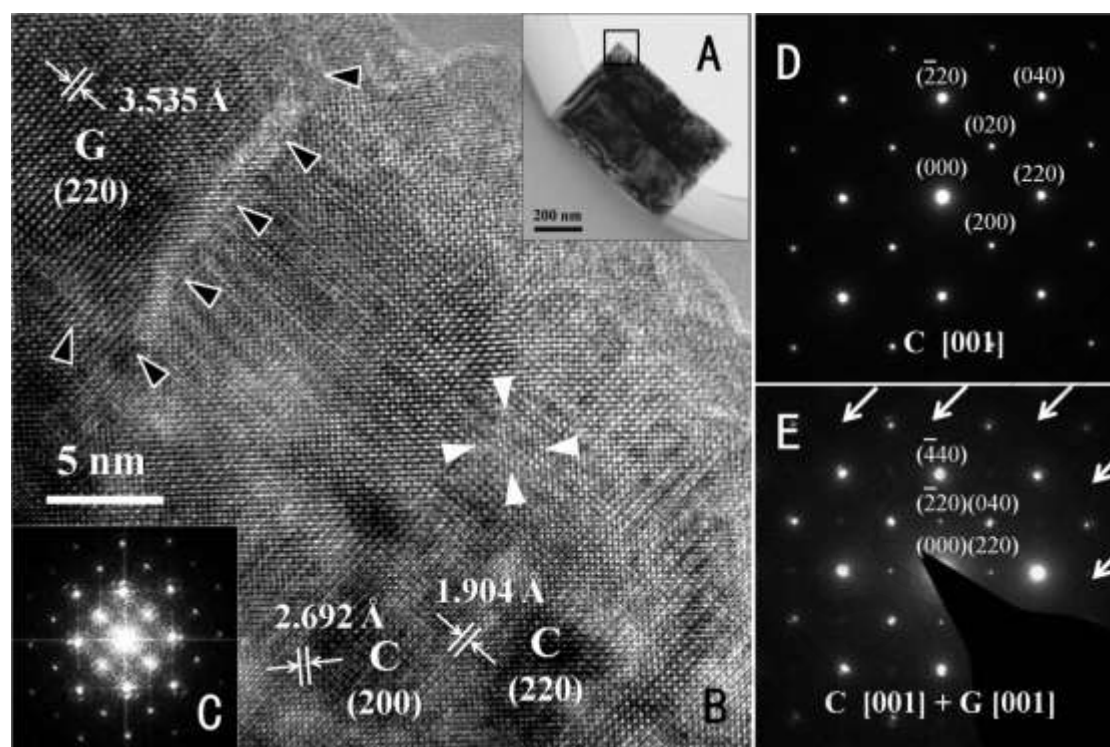


Figure 13:

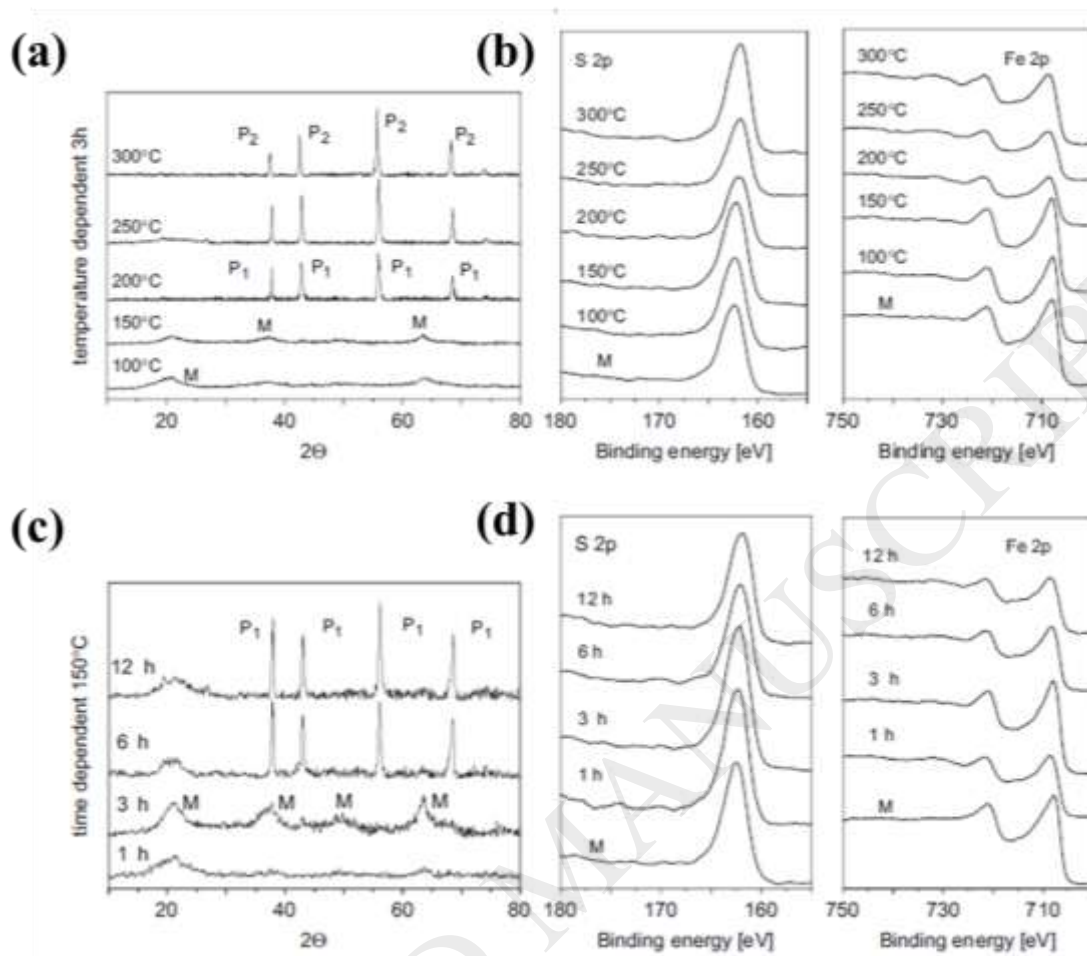


Figure 14:

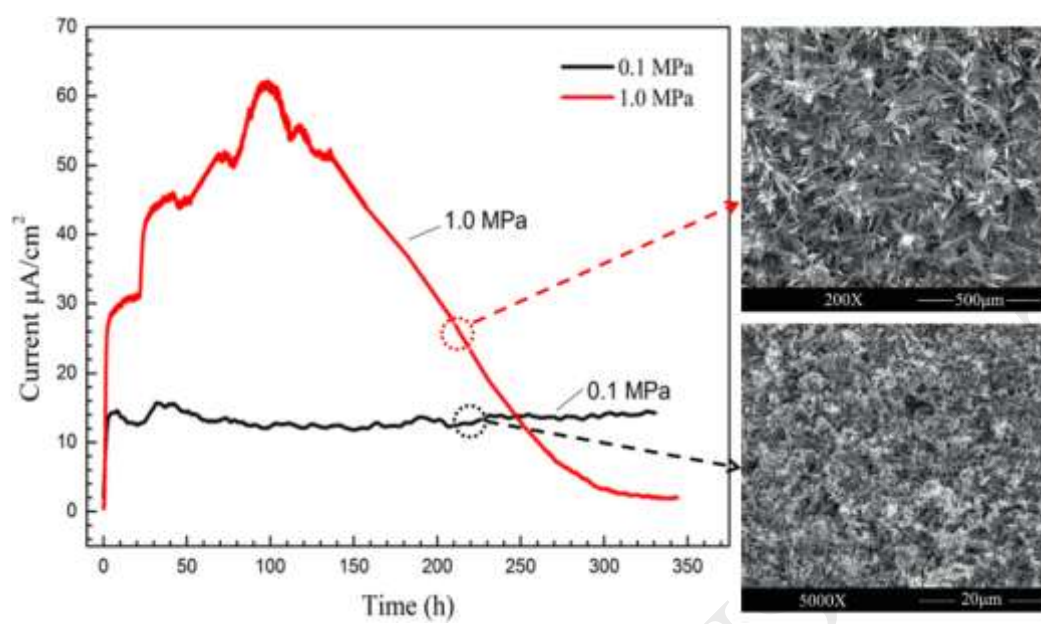


Figure 15:

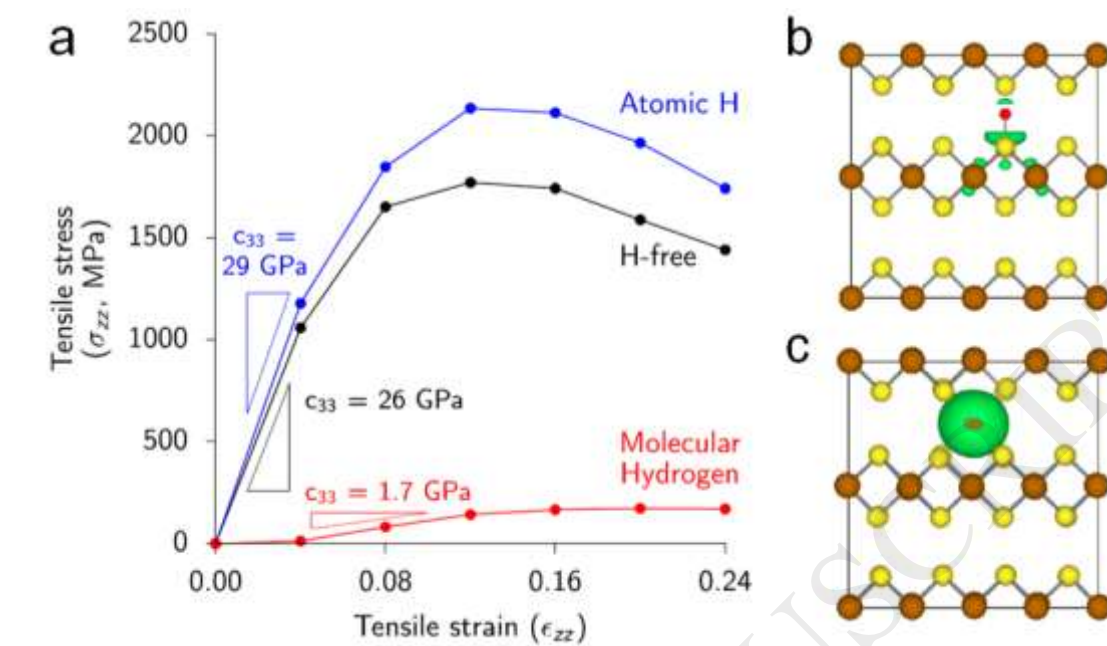


Figure 16:

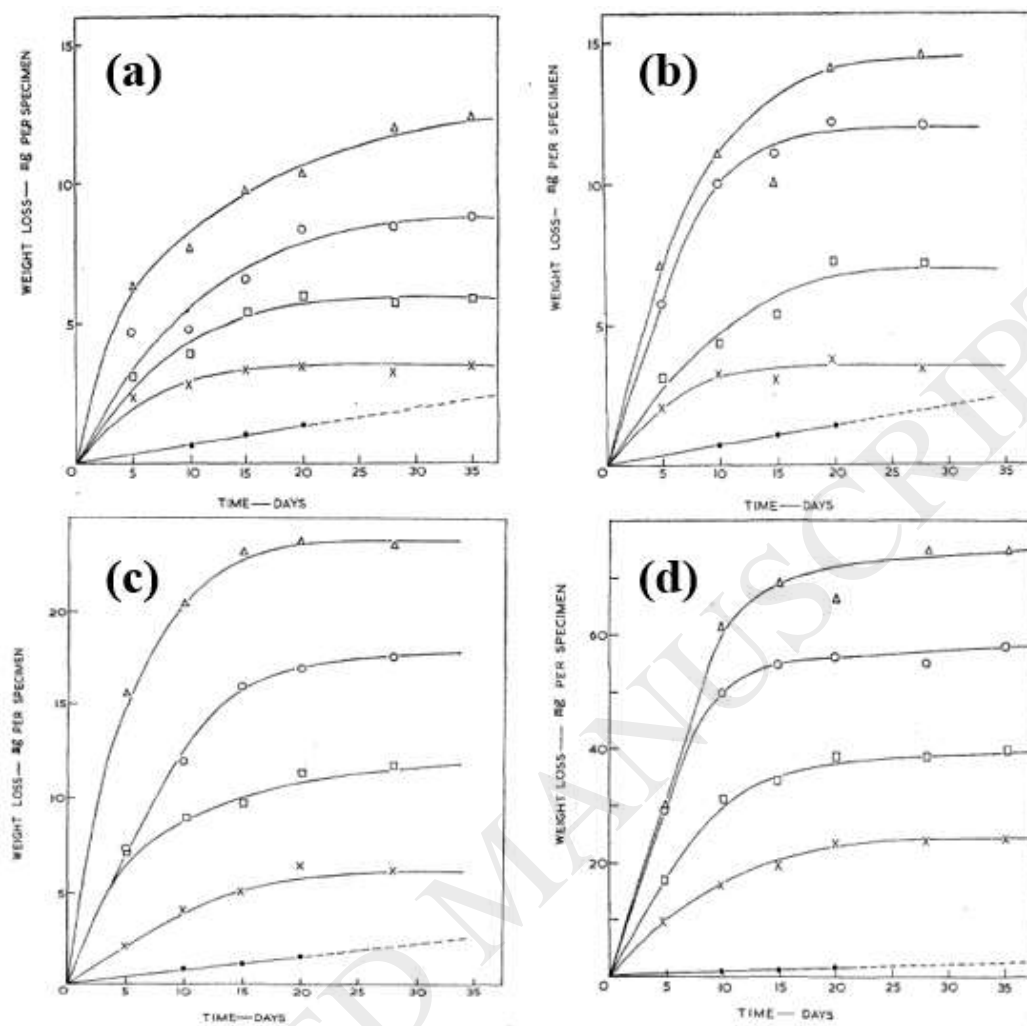


Figure 17:

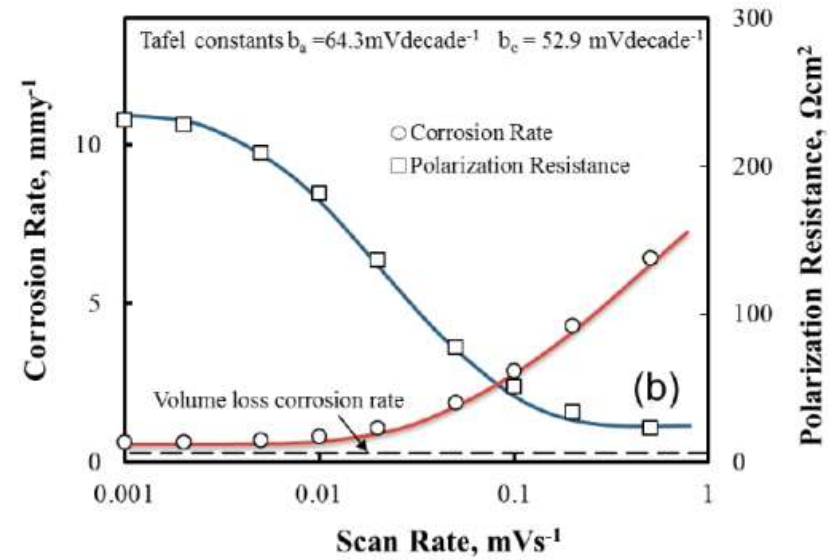
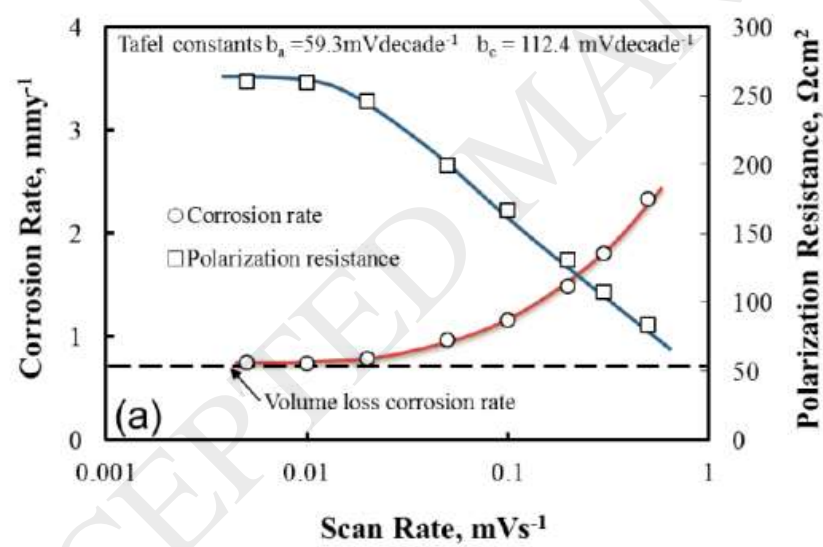


Table 1: Solid-phase iron sulphide compounds. Reproduced from Rickard [45] with permission from the American Chemical Society (ACS).**Table 1:**

Material	Composition	Lattice structure	Properties	Natural distribution
Amorphous FeS	Fe(HS) ₂ , FeS _x	Non-crystalline	Metastable	Unknown
Mackinawite	Fe _{1+x} S, x = 0.005-0.025	Tetragonal: <i>P4/nmm</i>	Metastable material; the major constituent of FeS precipitated from aqueous solutions.	Widely distributed in low-temperature liquid environment.
Cubic FeS	FeS	Cubic: <i>F$\bar{4}3m$</i>	Highly unstable phase	Not found naturally
Troilite	FeS	Hexagonal: <i>P$\bar{6}2c$</i>	Stoichiometric end member of the Fe _{1-x} S group.	Mainly found in meteorites.
Pyrrhotite	Fe ₇ S ₈ , Fe _{1-x} S	Monoclinic: <i>A2/a</i> ; hexagonal: <i>P6/mmc</i>	When x > 0.2, it is non-stoichiometric steady-state phase; the monoclinic structure is about Fe ₇ S ₈ ; and the hexagonal structure is approximately Fe ₁₀ S ₁₁ .	Iron sulphides in the Earth and solar system; rare in marine systems.
Smythite	Fe ₉ S ₁₁ , Fe ₇ S ₈	Hexagonal: <i>R3m</i>	Metastable phase related to the Fe _{1-x} S group.	As a rare mineral, it is mainly found in hydrothermal systems, often associated with carbonates.
Greigite	Fe ₃ S ₄	Cubic: <i>Fd3m</i>	Metastable Fe ²⁺ , Fe ³⁺ sulphide; the thiospinel of iron	Particularly associated with fresh water systems.
Pyrite	FeS ₂	Cubic: <i>Pa3</i>	Stable iron (+2) disulphide known as “fool’s gold”	The most abundant sulfide on the Earth’s surface.
Marcasite	FeS ₂	Orthorhombic: <i>Pnnm</i>	Metastable iron (+2) disulphide	Common mineral hydrothermal systems and sedimentary rocks.

Table 2: Different types of H₂S corrosion products and the corresponding experimental parameters [33, 50, 51, 61, 78, 79, 81-89].

Table 2:

Experimental parameters					Corrosion product					Author
<i>t</i>	<i>T</i>	<i>p</i> H ₂ S	<i>p</i> CO ₂	Cl ⁻	Mackinawite	Troilite	Cubic FeS	Pyrrhotite	Pyrite	
5 h					√					Benning et al. [33]
24 h	25 °C	99.5%			√					
66 h					√				√	
120 h	50 °C	10.0%			√					
192 h			N	N	√					
24 h		99.5%			√					
264 h	80 °C	/							√	
96		50.0%			√					
24 h	95 °C	/							√	
173 h		50.0%			√					
5 h					√					Bai et al. [50]
1 d	50 °C	/	N	N	√					
4 d					√		√			
6 h							√			Bai et al. [51]
72 h	50 °C	1.0 MPa	N	N		√				
		0.3 MPa	0.18 MPa		√					Zhang et al. [61]
120 h	60 °C	1.0 MPa	0.59 MPa	N	√			√		
		1.5 MPa	0.88 MPa		√	√		√		
96 h		1.2 MPa	0.60 MPa		√					

216 h	90 °C	1.5 MPa	0.20 MPa		√	√		√	
8 h	85 °C	0.1 MPa	N	N	√	√		√	√
4 d	42 °C							√	
65 h	25 °C	0.1 MPa 0.22 MPa	N	N				√	
2.7 h					√				
3.5 h	35 °C	1.5 MPa	N	N			√		
72 h						√			
20 h	218 °C	1.34 MPa	bal Ar	Y				√	
240 h			Ar					√	
24 h	95 °C	0.02 MPa	N	Y				√	
30 d		0.002 MPa	0.2 MPa					√	
138 h	120 °C	0.28 MPa		Y				√	
166 h			0.69 MPa					√	
383 h		0.35 MPa						√	
72 h	100 °C	0.01 MPa 0.02 MPa	1.7 MPa	Y	√			√	
6.4 y	110 °C	0.564 MPa	0.60 MPa	Y				√	
8.6 y		0.855 MPa	0.58 MPa					√	
9 d	130 °C	0.108 MPa	N	N				√	
12 d									√
120 h	60 °C	2 MPa	1.17 MPa	Y				√	
72 h	60 °C	0.3 MPa			√				
96 h	120 °C	1.2 MPa	N	N			√	√	
	150 °C					√		√	

120 h	60 °C	0.3 MPa		√		
	130 °C	3 MPa	√		√	
216 h	90 °C	1.5 MPa	√		√	√

Table 3: Corrosion rates of the different corrosion products [123-128].

Table 3:

Corrosion product	Corrosion rate (mm/year)	Author
FeS (1 mm)	0.74	Wallaert et al. [123]
FeS (5 mm)	0.31	
FeS (mackinawite)	0.20	Sherar et al. [124]
FeS	0.21-1.18	Miranda et al. [125]
FeS	0.35-0.50	Gayosso et al. [126]
FeS	0.67	Fatah et al. [127]
FeS (mackinawite)	5.30	Edyvean et al. [128]
Greigite	119.60	